A Study of Carbon Dioxide Capture and Catalytic Conversion to Methane using a Ruthenium, "Sodium Oxide" Dual Functional Material: Development, Performance and Characterizations

Shuoxun Wang

Submitted in partial fulfillment of the
requirements for the degree of
Doctor of Philosophy
in the Graduate School of Arts and Sciences

COLUMBIA UNIVERSITY

2018

ABSTRACT

A Study of Carbon Dioxide Capture and Catalytic Conversion to Methane using a Ruthenium, "Sodium Oxide" Dual Functional Material: Development, Performance and Characterizations

Shuoxun Wang

The increasing CO_2 level in the atmosphere, mostly attributed to anthropogenic activities, is overwhelmingly accepted to be the main greenhouse gas responsible for climate change. Combustion of fossil fuel is claimed to be the major cause of excess CO_2 emission into the atmosphere, but human society will still rely heavily on fossil fuel for energy and feedstock supplements. In order to mitigate the environment-energy crisis and achieve a sustainable developing mode, Carbon Capture, Utilization and Storage (CCUS) is an effective method and attracts considerable interests.

Rather than conventional aqueous amine-based liquid absorbent, e.g. the toxic, corrosive and energy intensive monoethanolamine (MEA), solid adsorbents are preferable for CO_2 capture. CO_2 utilization via CO_2 conversion to fuel or other value-added products is favored over CO_2 storage. Also it is preferred that no transportation of captured CO_2 is required. Capturing and converting CO_2 to fuel, such as synthetic natural gas or CH_4 is particularly useful if it is produced at the site of CO_2 generation. The converted CO_2 can then be recycled to the inlet of the power plant or integrated into existed fuel infrastructure eliminating any transportation.

This thesis presents a study of the development, performance and characterizations of a newly discovered (second generation) dual functional material (DFM) for CO_2 capture and catalytic conversion to methane in two separated steps. This material consists of Ru as the methanation catalyst and "Na_2O" obtained from Na_2CO_3 hydrogenation as the CO_2 adsorbent, both

of which are deposited on the high surface area γ-Al_2O_3 support. The Ru, "Na_2O" DFM captures CO_2 from O_2- and steam-containing flue gas at temperature from 250 °C to 350 °C in step 1 and converts it to synthetic natural gas (CH_4) at the same temperature with addition of H_2 produced from excess renewable energy (solar and/or wind energy) in step 2. The heat generated from methanation drives adsorbed CO_2 to Ru by spillover from the adsorption sites and diffuse to Ru for methanation. This approach utilizes the heat in the flue gas for both adsorption and methanation therefore eliminating the need of external energy input.

The second generation DFM was developed with a screening process of solid adsorbent candidates. Initial adsorption studies were conducted with powdered samples for CO_2 capture capacity, methanation capability, and resistance to an O_2-containing simulated flue gas feed. The new composition of DFM was then prepared with tablets for future industrial applications and scaled up to 10 grams suitable for testing in a fixed bed reactor. Parametric and 50-cycle aging studies were conducted in a newly constructed scaled-up fixed bed reactor using 10 grams of DFM tablets in the simulated flue gas atmosphere for CO_2 capture.

With the presence of O_2 in CO_2 feed gas for step 1, the Ru catalyst is oxidized but must be rapidly reduced in step 2 to the active metallic state. Parametric studies identified 15% H_2 is required for stable operation with no apparent deactivation. The parametric plus 50-cycle aging studies demonstrated excellent stability of the second generation DFM.

A kinetic study was also conducted for the methanation step using powdered DFM but prepared via the tablet method to minimize any mass transfer and diffusion influence on the methanation rate. An empirical rate law was developed with kinetic parameters calculated. The methanation rate of captured CO_2 is highly dependent on H_2 partial pressure (approaching a

reaction order of 1) while essentially zero reaction order of CO_2 coverage was determined. The kinetic study highlights the importance of H_2 partial pressure on the methanation process.

Characterizations were conducted on the ground fresh and aged (underwent parametric and aging studies) DFM tablets. BET surface area, H_2 chemisorption, X-ray diffraction (XRD) pattern, transmission electron microscopy (TEM) images and scanning transmission electron microscope-energy dispersive spectroscopy (STEM-EDS) mapping were utilized to study the material changes between fresh and aged samples. From fresh to aged, similar BET surface area was measured, improved both Ru and "Na_2O" dispersion, and decreased Ru cluster size was observed while no definitive proof of the nature of the sodium species was obtained via XRD.

The second generation DFM containing 5% Ru, 6.1% "Na_2O" / Al_2O_3 was shown to possess the capability of capturing CO_2 from O_2-containing simulated flue gas and subsequent methanation with addition of H_2 produced from excess renewable energy (or from chemical processes) with twice the CO_2 and CH_4 capacity relative to the first generation DFM. Activity, selectivity and stability has been demonstrated for the second generation DFM.

We envision swing reactors to be utilized commercially where the flue gas feed for step 1 and H_2 for step 2 are throttled alternatively between each reactor for continuous operation.

Table of Contents

List of Figures

List of Tables

Acknowledgements

I would like to extend my sincere gratitude to my advisor Prof. Robert J. Farrauto for all his guidance, support, encouragement and concern throughout my entire Columbia experience for both Master and PhD studies. Bob is not only a professional coach to me, but also a life mentor, who has given me countless instruction and advice for my career and life philosophy. He introduced catalysis to me in my first year at Columbia and inspired my passion for this subject, and consequently I hope this will be a major part of my future career. His constant patience and critical opinions provided a path for my research experience. I have been very fortunate to have him as my supervisor, mentor and friend for life.

I would also like to express my heartfelt thanks to my esteemed committee members, Prof. Ah-Hyung (Alissa) Park, Prof. Ngai Yin Yip, Prof. David Vallancourt and Dr. Michel Deeba for following my research over these years and always offering vital feedback. It has been my great honor to have the opportunity to learn from these expert scientists.

My acknowledgements also go to all the former and present group members of the *Catalysis for a Sustainable Environment* research group: Dr. Melis S. Duyar, Dr. Qinghe (Angela) Zheng, Dr. Emi Leung and Ms. Martha Arellano. It was their care, help, cooperation and companionship that made me feel loved and positive during these years' research. I would also like to thank Mr. Erik T. Schrunk, Mr. Ji Ho Jeon, Mr. Sam Karp, Mr. Daniel M. Eida and Ms. Kelly Conway for their assistance in my research. They are just a few of the wonderful people I have met in New York and are not only colleagues but extended family to me.

I'd also like to thank Ms. Elizabeth Allende, Ms. Karen Del Aguila, Ms. Marietta Bell and Ms. Hong Yuan for their consistent help during my studies. Furthermore, I would like to thank all

my friends that I was lucky enough to meet, especially those at Columbia, Xi Chen, Hanqing Fan, Zhuoran Zhang, Jingsui Wang, Shannon M. Hubbard, Ming Gao, Haowei Zhai and Xiangbiao Liao for their love, care and patience which has made New York a life-long happy memory for me.

I'd like to offer my sincere thanks to Anglo American Platinum for their generous and persistent financial and personal support for my thesis research.

Finally, I would like to dedicate this thesis to my family, especially my parents Guomei Chen and Jinbo Wang for their infinite love, support and encouragement that fostered me with a positive personality and enhanced my self-confidence allowing me to achieve this wonderful goal.

To my parents Guomei and Jinbo

Chapter 1: Introduction

1.1 Motivation

As early as 1995, the Intergovernmental Panel on Climate Change (IPCC) had concluded in their second assessment report that human activities were contributing to the global climate change [1]. Since then, numerous independent studies have reached the scientific consensus that anthropogenic emission of greenhouse gases (GHG) is responsible for the increasing global temperature and climate change. Carbon dioxide (CO_2) is the primary GHG, that traps radiant energy within the thermal infrared range in the atmosphere, emitted by anthropogenic activities with an increasing trend. The effects of increased CO_2 levels in the atmosphere on various aspects from agriculture [2] to marine life [3], the economy [4], etc. are now well known. The Conference of the Parties (COP21) in Paris 2015 agreed for the first time that both developed and developing countries need to reduce GHG emissions [5]. This requires more ambitious emission reduction targets and higher levels of cooperation and development of technology, economy and policy.

A major emission source of CO_2 from anthropogenic activities is fossil fuel combustion, accounting for 76.3% of the emissions from liquid and solid fossil fuel [6]. Currently, global energy infrastructure still relies heavily on fossil fuels for its energy supply. An agreement to maintain the global temperature warming below 2 °C above the average global temperature of pre-industrial times was achieved in the 2009 United Nations Framework Convention on Climate Change (UNFCCC) Conference [7]. To meet this target, a third of oil reserves, half of gas reserves and over 80% of current coal reserves should remain unexploited from 2010 to 2050 [8]. With expected population and economic growth, the ever-increasing energy demand poses a number of challenges for balancing human civilization development and global climate change control.

Renewable energies such as solar and wind energy are popular alternative resources for people to adapt for zero-emission credits. Renewable energies possess enormous potential to be the new energy supplement for carbon neutral development but the inherit intermittence and geographical dependence limit their implementation and application. Hydrogen gas production via water electrolysis powered by renewable energies works as an energy storage method. The H_2 generated can be easily compressed and transported. Hydrogen is a green fuel itself but also a key feedstock for carbon-containing sources for fuel.

Carbon Capture, Utilization and Storage (CCUS) was proposed to achieve a carbon neutral society, encompassing methods and technologies to remove CO_2 from the atmosphere and the flue gases followed by recycling the CO_2 for conversion to useful products or by safe and permanent storage. To reach the goal of reducing the rising atmospheric CO_2 concentration while meeting the increasing energy demand, a comprehensive portfolio of technologies exists and needs to be deployed for the long term [9]. CO_2 would become an easily and widely available feedstock for fuel and chemical production, if efficient and sufficient CCUS technologies can be developed and implemented. Using renewable energy for power and products, a carbon neutral economy can be achieved.

Much research has led to the development of CCUS technologies for a wide range of applications. A finite-element mathematical simulation model was developed to assess the CO_2 adsorption into promoted hot potassium carbonate present in hollow fiber membrane contactors (HFMCs) with enhanced performance compared to commonly used liquid amines [10]. CO_2 separation from a CH_4 gas stream was investigated using a co-polymer composite membrane consisting of PVC operating at low temperatures and CO_2 partial pressures were found to have negative correlations with the selectivity of CO_2 permeation through the membrane [11].

Thermodynamics requires high pressure to directly hydrogenate CO_2 from post-combustion effluent to produce methanol, but catalysts would allow low temperature for manufacturing such products once oxygen is removed from the gas feed [12]. Injected CO_2 enhanced oil recovery (CO_2 EOR) is considered the most practical method for producing liquid oil with the associated gas being recycled [13].

Currently the most popular and efficient method for CO_2 capture is to scrub CO_2 off gas streams using amine-based solvents. The adsorbent, monoethanolamine (MEA), is toxic and corrosive and thus must be diluted with 70% ~ 80% weight of water. The separation of CO_2 from the aqueous amine experiences a large energy penalty due to endothermic water volatilization [14]. This renders unfavorable economic challenges which accounts for 70% ~ 80% of the full cost of CCUS processes [15]. Furthermore, the CO_2 must then be transported to a geological sequestration site and/or to a process for further catalytic upgrading. Catalysts for the direct synthesis of methanol, from only CO_2, lose selectivity at high conversions. It is common commercial practice to add up to 15% CO_2 to H_2 and CO mixtures for the synthesis using a CuZnAl catalyst [16].

This thesis focuses on comprehensively addressing the demand of sustainable energy development and the necessity to reduce the carbon dioxide concentration in the atmosphere, as these are the two effective strategies in dealing with current environmental issues. This current work advances a Dual Function Material (DFM), that captures and catalytically converts CO_2 from a simulated natural gas power plant effluent to a useful fuel. The two-step process occurs at atmospheric pressure, at flue gas temperature, with no external heat addition needed. The hydrogen is provided by electrolysis of water from excess wind or solar energy. The product methane (synthetic natural gas or SNG) is dried and recycled to the inlet of the power plant for reuse. This

decreases the amount of natural gas that must be extracted from the earth while mitigating the emission of CO_2 to the atmosphere using stored renewable H_2.

The DFM contains a hydrogenation catalyst (Ru for methanation) and a reversible CO_2 adsorbent (CaO or "Na_2O") both supported on a high surface area carrier (γ-Al_2O_3). The alkaline sites saturated with CO_2 are exposed to H_2 from renewable energy for methanation catalyzed by Ru. The heat generated from the exothermic methanation reaction desorbs the CO_2 where it "spills over" to the Ru sites to complete methanation. One can envision the commercial process operating with swing reactors where one is capturing CO_2 while the second is undergoing methanation. The system is then reversed for continuous operation.

The initial DFM was designed with Ru and CaO deposited on a γ-Al_2O_3 support [17]. However, the production of methane is limited by low CO_2 adsorption of supported CaO. The second generation DFM with a larger capacity adsorbent, designated as "Na_2O", is produced by the H_2 pre-treatment of supported Na_2CO_3 on γ-Al_2O_3 [18]. In this thesis, DFM technology is expanded to include the higher capacity adsorbent, advanced aging studies demonstrating stability and more detailed kinetics of the methanation step.

1.2 Thesis Structure

This work aims to present a thorough laboratory study of the Ru, "Na_2O" DFM demonstrating scale up from powders to tablets, process parameters, aging performance in a simulated power plant flue gas, characterization for fresh and aged samples and a kinetic analysis of the key variables necessary for scale up.

An overview of the background and existing literature related to climate change and carbon neutralization, CO_2 capture technologies, CO_2 utilization technologies, CO_2 methanation,

renewable energy implementation and published DFM research is presented in chapter 2. This chapter is composed of the global environmental and energy issues and highlight the weaknesses of the current state of the art CCUS technologies. A summary of previous achievements of the DFM technology acts as the background for this study.

Detailed experimental methods and equipment used to investigate the second generation DFM feasibility in flue gas applications and its performance, stability, etc. are presented in the third chapter. The specific test protocols and thorough explanation of experimental details are included in the corresponding chapters that follow chapter 3.

The preparation, performance and stability of the second generation DFM was preliminarily determined in the powder form via thermogravimetric analysis (TGA) tests. The results of these powder studies are presented in chapter 4 where hydrogen intensity (exposure time) is stated to be necessary to maintain activity of the DFM.

Chapter 5 focuses on the short-term cyclic tests in a scaled-up fixed bed reactor with newly prepared DFM tablets. Two sets of cyclic tests were conducted in diluted CO_2 feed gas and simulated flue gas. The results indicate that the DFM technology is feasible for applications in the O_2- and steam-containing simulated flue gas and emphasizes the importance of H_2 intensity in maintaining stable performance.

An empirical rate law for the adsorbed CO_2 methanation process using the powdered DFM (via $RuCl_3$) was developed. Kinetics were conducted with powdered DFM to minimize any mass transfer or diffusion influence on the methanation rates. The empirical rate law showed that the methanation rate of the adsorbed CO_2 depends on H_2 partial pressure while the CO_2 coverage on the material surface appears to have no effect on the rate. Details are presented in chapter 6.

Chapter 7 describes the parametric study using tablet DFM (5 mm × 5 mm) in simulated flue gas to provide guidance for industrial application conditions. Parameters of feed gas hourly space velocity, process temperature and CO_2 adsorption duration time (i.e. O_2 exposure of Ru) were studied. This study provides guidance for cyclic aging and eventually continuous operation using on a swing reaction system.

Chapter 8 provides the data generated demonstrating DFM stability using 50 cycles of CO_2 adsorption and methanation, together with the characterizations for fresh and aged DFM tablet samples.

Finally, chapter 9 presents the conclusions and suggested future work.

Chapter 2: Background and Literature review

2.1 Climate Change and Carbon Neutral Society

Climate change is an inevitable global issue substantiated by evidence of global temperature rise [19], warming oceans [20], shrinking ice sheets, glacial retreat [21], declining Arctic sea ice [22], sea level rise [23], etc. Millions of people from developing countries flee every year from drought and famine incurred by climate-related crises. Climate change will likely create political violence and civil wars as critical resources become scarce [24].

Carbon dioxide (CO_2) is widely acknowledged as the major greenhouse gas and its rising level in the atmosphere contributes to global warming and climate change issues. Combustion of fossil fuel claims the major part of anthropogenic CO_2 emission creating serious consequences to the carbon cycle. A number of emerging studies have aimed at developing a carbon neutral society using alternative technologies for thermal energy [25], transportation [26], buildings [27], electricity [28], etc.

It is highly unlikely a single technological invention will independently solve the global energy-environment crises. Dealing with such a complex problem requires a high level of cooperation politically and economically with comprehensive applications of various technological innovations. While zero-emission renewable energies such as solar and wind energy are deployed more widely, carbon capture and utilization technologies are still necessary to mitigate the increasing level of atmospheric CO_2 due to the dependence on fossil fuel.

2.2 CO_2 Capture Technologies

In the past decades, CO_2 capture technologies have stimulated a lot of research in pre- and post-combustion capture and oxy-fuel combustion capture [29, 30]. Post-combustion capture is

one of the key technologies that can be potentially retrofitted into the existed industrial infrastructures without operational interference of their processes and energy supplies.

Conventional amine-based liquid CO_2 scrubbing technologies are strongly considered for use in commercial processes because it is proven to successfully treat industrial effluent gas streams. However, such aqueous amine systems are costly and energy intensive. The cost of CO_2 capture using this technology for 90% of CO_2 mitigation from flue gas of power plants will be \$40~100 / ton of CO_2 equivalent to about 30% of the power produced [31]. Because of this, other more efficient technologies are being pursued.

Solid adsorbents, capable of CO_2 capture from flue gas streams show many potential advantages over the conventional amine-based liquid CO_2 scrubbing technology. They have been extensively studied however, they operate at low temperatures and require elevated temperatures for separation of CO_2 from the adsorbent [32].

Physi-sorbent materials are candidates including porous carbonaceous materials, zeolites, alumina and metal-organic frameworks (MOFs) [32]. In 1998, activated carbon was studied theoretically and experimentally for its CO_2 adsorption ability at varying temperatures [33]. Activated carbon still is of interest for its capability of CO_2 capture from flue gas [34, 35]. Metal-organic framework (MOFs) materials are a relatively new class of solid sorbents under consideration. Their pore size, pore shape, extremely high internal surface areas and potential for chemical modification via varying organic linkers allow the manipulation of selectivity, kinetics and capacity [32]. CO_2 uptake capacity reached 2400 mg / g at room temperature and ~50 atm. [36]. Capture capacity of physical sorbents rely heavily on temperature and pressure, thus are not favorable for industrial applications where flue gases are at atmospheric pressure and high

temperature, requiring compression and cooling. Also, physi-sorbents suffer from low selectivity toward CO_2 and low CO_2 uptake capacities at relatively low CO_2 partial pressure.

Chemisorbents, with modifications to their surface chemistry, can be prepared with basic sites for acidic CO_2 adsorption enhancing CO_2 capture capacity and high selectivity for CO_2. Alkali-metal carbonates are primary candidates because of their commercial feasibility and inexpensive availability [37]. Supported Na_2CO_3 and K_2CO_3 were studied for their CO_2 capture capacities at low temperatures with regeneration requiring temperature swings from 60~100 °C to 120~220 °C or higher [38-52]. Enhanced CO_2 adsorption was observed in ammonia treated commercial activated carbon at higher temperatures (200 °C) attributed to the introduction of nitrogen-containing groups to the carbon structure [53]. An aminated zeolite also showed improvement in CO_2 adsorption capacity at 120 °C with 50% MEA (monoethanolamine) where chemical absorption is dominant [54, 55]. Although amine-treated absorbents showed enhanced performance, such materials are still not feasible for in situ CO_2 capture due to toxicity, corrosion and negative interactions with the O_2 present in flue gases.

Hollow fiber membranes are emerging technologies for CO_2 capture. The most commonly used hollow fiber membrane materials are polypropylene (PP), polyethylene (PE), polytetrafluoroethylene (PTEE), polyetherimide (PEI), etc. [56]. However, critical obstacles for wide scale application of membrane technology are still questionable due to issues with inadequate wetting of the liquid adsorbent throughout membrane pores [57].

Studies have been considered combing two or more approaches for the CO_2 capture processes. Four types of hybrid CO_2 capture processes have been studied; absorption based [58-60], adsorption based [61-65], membrane based [66-68] and cryogenic based [69-72] systems. Such research is still at its laboratory infant stage. Furthermore, the CO_2 concentration is limited

to 15% or higher (approximately twice that of a natural gas power plant effluent CO_2 content) and operational conditions are not suitable for many industrial effluent situations [73].

2.3 CO_2 Conversion and Utilization Technologies

CO_2 conversion and utilization is a promising pathway to mitigate the environmental crises caused by excessive CO_2 emissions. Much effort is currently in progress to convert CO_2 via catalytic hydrogenation processes to various value-added hydrocarbon products such as methanol or methane. The addition of H_2, produced from renewable energies, is considered a potential sustainable path toward a carbon neutral manufacturing process for hydrocarbon fuels. Thermal chemical, electrochemical and photochemical catalysis are three interesting approaches.

Catalysts for CO_2 hydrogenation are being intensively studied in laboratories for conversion to CH_4, lower olefins [74], higher hydrocarbons [75], formic acid [76], methanol [77-79], higher alcohols [80], etc. Heterogeneous catalysts offer several technical advantages such as low energy consumption, stability, selectivity, products separation, reuse of the catalysts and simple reactor design [81]. Renewable hydrogen is a key reactant for such processes. Challenges in selectivity and life still remain before commercialization can be realized.

Rather than store and transport the hydrogen generated via water electrolysis powered by renewable energies, one can utilize the electricity produced by solar and/or wind energies directly for CO_2 conversion through electrochemical catalysis. For successful commercialization, both high efficiency (often > 95% selectivity) for a desired product and sufficient current density are required [82]. In an electrolyzer, CO_2 is reduced into desired products on the cathode while the oxygen evolution reaction (OER) occurs on the anode. See Equation 2.1~2.4 for the examples of the half-reactions on the cathode [82]. Metal catalysts of Au, Ag, Pt, Ti, Ni, etc. [83-89] have been

studied. However, the current density for the state of the art of electrolysis cells providing (~100 mA / cm^2 [90]) is still far from sufficient for large scale applications. Therefore, significantly improved electro-catalysts are needed [82].

$$CO_2 + 2H^+ + 2e^- \rightarrow CO + H_2O \quad \text{(Equation 2.1)}$$

$$CO_2 + 8H^+ + 8e^- \rightarrow CH_4 + 2H_2O \quad \text{(Equation 2.2)}$$

$$2CO_2 + 12H^+ + 12e^- \rightarrow C_2H_4 + 4H_2O \quad \text{(Equation 2.3)}$$

$$CO_2 + H^+ + 2e^- \rightarrow HCOO^- \quad \text{(Equation 2.4)}$$

CO_2 photo-reduction can utilize solar energy directly to convert CO_2 to chemicals or fuels to achieve the CO_2 neutralization goal. There are three major steps: solar light harvesting, charge separation and transportation, and surface reactions [91]. The first two steps have been optimized significantly as they are related to the same solar-driven water splitting issues [92-100], while research dedicated to improving the third is needed [101, 102]. Although achievement and improvements have been made, the stability of photocatalysts is still poor in aqueous electrolytes. As suggested by Chang et al. [91], possible approaches to deal with this issue for future large-scale applications can be coating surface protective layers with advanced techniques, such as electron beam evaporation and sputter deposition.

CO_2 injection for enhanced oil recovery (EOR) technology is the most significant method for CO_2 utilization which is being successfully demonstrated for varying oil reservoirs. Since the first CO_2 immiscible flooding was deployed in 1968 [103], a considerable number of such projects have been undertaken in many countries and more are taking place. The incremental production

of oil by 4.7% ~ 12.5%, 8.5% on average, was obtained and a production rate per well of 23.0 bbl / d / well was achieved [104]. Some operational problems cannot be avoided such as early gas breakthrough, injectivity reduction and generation of hydrogen sulfide [104].

2.4 CO_2 Methanation

The Sabatier reaction, see Equation 2.5, was first reported by the French chemist Paul Sabatier in 1902 [105], which provides the theoretical foundation for CO_2 methanation. This is an exothermic process with high equilibrium conversion within the temperature range from 25 °C to 400 °C [106, 107]. In the presence of proper catalysts, CO_2 methanation can be complete with over 99% CH_4 selectivity thereby avoiding product separation [108]. The concept of "power to gas" (PtG) has gathered considerable attention whereby CO_2 (from landfills) and H_2 from renewable energies catalytically produce CH_4 as an alternative source of synthetic natural gas [108]. This technology has been advanced by Audi in Germany [109].

$$CO_2 + 4H_2 \rightarrow CH_4 + 2H_2O \qquad \Delta H = -165.0\ kJ/mol$$

(Equation 2.5)

CO_2 methanation can be catalyzed by transition metals including Ru, Rh, Pt, Pd, Ni and Co [110-116, 17, 18] with an activity order of Ru > Rh > Ni > Pd > Co > Pt [117, 18]. Ni is a favorable catalytic metal due to its low cost and relatively good activity for industrial purposes, but it is easily oxidized and needs high temperature to be reduced. Thus, its application is limited to O_2-free environments.

Commonly used catalyst supports for CO_2 methanation are Al_2O_3, SiO_2, ZrO_2, TiO_2, CeO_2 and zeolites [118-123]. The support properties can influence the performance of the metal catalysts due to pore size, pore volume, surface chemistry and metal-support interactions. Different activity performance was observed from a series of Ni / CeO_2 catalysts with the same composition but prepared via hard- and soft-template methods, and precipitation method. These differences attributed to the mesoporous structure of the supports [124]. In addition, different support crystal phases also have an influence on catalyst performance. A sample composed of RuO_2 / TiO_2 showed varying activity and product selectivity depends on the crystal phases of TiO_2 [125].

Metal particle size also has a strong impact on the kinetic parameters. Wu et al. reported for a Ni / SiO_2 catalyst, with a metal loadings from 0.5 wt% to 10 wt% generated both small Ni clusters and large Ni particles resulting in CO formation on the small clusters while CH_4 production occurred on the larger particles [126]. A similar phenomenon was observed with a Ru / Al_2O_3 catalyst, where 1 wt% Ru had better metal dispersion and showed high production of CO while selectivity shifted to CH_4 with increased Ru metal particle size. CH_4 became the dominant product when the Ru loading increased (dispersion decreased) to 5% [113]. Experimental evidence indicated that, within a certain range of metal particle size, the atom-scale structured catalytic metal favors the reverse water gas shift (RWGS) reaction, while the larger particle structure prefers CH_4 production [116].

Multi-component doped metal catalysts are being studied for CO_2 methanation to optimize the metal redox property or to adjust the surface basicity for enhanced adsorption of CO_2 [108].

The mechanism of CO_2 methanation has been commonly suggested as occurring through two major routes, either CO or a formate route. The CH_4 selectivity is likely determined by the competition between hydrogenation and C-O bond generation from the intermediates of $*H_xCO$

[127]. A specific route for a certain catalytic CO_2 methanation process varies depending on the system used. For example, evidence from operando XANES, IR, DRIFTS and Raman analyses by Duan et al. indicated both Ru / CeO_2 and Ru / Al_2O_3 favored CO_2 methanation [128]. They reported that Ru / Al_2O_3 formed a carbonyl species with CH_4 generation, while for Ru / CeO_2 formate and methanol species were produced at 250 °C and 150 °C respectively. Another comparison was shown between Ru-substituted $Ce_{0.95}Ru_{0.05}O_2$ and a supported metal catalyst (Ru / CeO_2) [129] for CO_2 methanation. The former reaction proceeded following the steps of $CO_2 \rightarrow CO \rightarrow OCH_2 \rightarrow OCH_3 \rightarrow CH_4$, while the latter followed a $CO_2 \rightarrow CO \rightarrow HCOO^- \rightarrow C \rightarrow CH_4$ route.

Deactivation of the metal catalysts is mainly divided into two phenomena; chemical and physical. The reason for chemical deactivation depends on the catalyst composition and reaction conditions. For CO_2 or diluted CO_2 feed streams, deactivation usually is caused by the formation of a spinel structure for Co [108, 130]. For an O_2-containing feed gas, the loss of active sites occurs because of the metal oxidation as is the case for Ni catalysts. High operational temperatures may cause support and/or metal sintering and deactivation by decreasing either the internal surface area or active metallic sites. Physical deactivation is usually due to carbon deposition on the surface of the catalysts masking the sites thereby prohibiting adsorption of reactants. Carbon deposition can be avoided by increasing the H_2 / CO_2 ratio or addition of steam which gasifies the deposited carbon [108].

Kinetics of CO_2 methanation over a 10% Ru / Al_2O_3 catalyst was investigated [131]. The result is consistent with an Eley-Rideal mechanism where H_2 gas reacts with the adsorbed CO_2. An empirical rate equation was determined providing activation energy, pre-exponential factor and reaction orders for CO_2, H_2, CH_4 and H_2O using a differential reactor approach at 230 °C, see Equation 2.6. The equation shows significant dependence on H_2 partial pressure and a much

weaker CO_2 partial pressure dependence. This kinetics study was conducted with only supported Ru catalyst and not DFM sample. The presence of a CO_2 adsorbent and the Ru catalyst generates slightly different kinetic parameters as will be demonstrated in this thesis.

$$R_{CH_4,f} = 35.5 \times e^{-66100/(RT)} \times {p_{H_2}}^{0.88} \times {p_{CO_2}}^{0.34} \times {p_{CH_4}}^{-0.11} \times {p_{H_2O}}^{-0.23}$$

(Equation 2.6)

2.5 Renewable Energy and H_2 Production

Multiple benefits by use of renewable energy are well acknowledged including reduced emissions of CO_2 and other air pollutants, a sustainable energy supply and economic growth, energy security, etc. Increased published studies since 2008 indicate that countries' decision-making processes on renewable energy deployment have gained and retained attention of scholars. According to a review by Sener et al., economic, environmental and social issues were found to be factors driving the deployment of renewable energy sources with no significant barriers over the analyzed period of 2008 ~ 2017 [132].

In March 2017, 10 percent of all U.S. electricity generation was contributed by solar and wind renewable energies, reflecting a major achievement over coal, natural gas and nuclear power [133]. An emerging unique opportunity for renewable energy implementation are housing installations that have potential large-scale application reducing the social and financial costs [134]. Renewable energy possesses large potential to be widely implemented, however, current uses are limited by their inherent intermittency, and require scalable means of storage [131]. H_2 generation, from water electrolysis powered by renewable energy, is a promising method to store the

intermittent energy while providing the key feedstock for CO_2 conversion and utilization to achieve a carbon neutral society.

Wind to power conversion is considered the lowest life cycle greenhouse gas analysis of all hydrogen production. This has been extensively studied [135]. This study utilized a modified Weibull probability distribution to reflect the actual range of wind speeds and wind energy density, and also provided the Levelized cost of hydrogen production with wind energy. The estimated supply cost of wind generated electricity is \$0.0844 ~ \$0.0864 kW h and renewable hydrogen production is \$5.30 ~ \$5.80 / kg-H_2.

H_2 production using photovoltaic (PV) power has been advanced by new PV systems that are more affordable compared to traditional ones [136]. However, PV energy is still far from being able to challenge fossil fuel electricity as the efficiency of these cells in commercial applications is only 10% ~ 20% although 29% has been reached by new developments [137]. Take a power station in the city of Yazd, Iran, for an example, 12.32% of the incoming solar radiation was converted into electricity from July 2012 to June 2012, which translates to 35.85 MWh of AC power with the potential of producing about 373 t of hydrogen gas per year [138].

2.6 Dual Functional Materials (DFM)

Instead of collecting CO_2 from either flue gases or the atmosphere followed by transportation to utilization and/or storage sites, integrating the CCUS units into power plants would decrease the energy / cost input significantly. Dual functional materials (DFM) were designed to offer a unique CO_2 capture and conversion to fuel solution relative to the CCUS concept. The DFM captures CO_2 from industrial effluents and catalytically converts the adsorbed CO_2 at the effluent temperature using renewable H_2. Thus, no external energy needs to be added

and the entire process is conducted at the site of CO_2 generation eliminating the need for transporting the CO_2. It utilizes renewable energy to convert CO_2 to synthetic natural gas that can be either recycled to the front end of the power plant or integrated into an existed natural gas infrastructure. Thus, it closes the carbon cycle.

Supported calcium oxide (CaO) was first discovered to have the capability of reversibly adsorbing CO_2 at 300 °C and desorbing it during a partial pressure swing at 300 °C [139]. Ru / Al_2O_3 showed excellent stability and selectivity to CH_4 for CO_2 conversion at 320 °C [140]. These two discoveries were the basis for the DFM invention [17]. DFM contains a CO_2 adsorbent and a catalyst both supported on high surface area carrier to capture CO_2 and convert it to methane without requirement of temperature swing. The initial DFM was designed with CaO and Ru functioning as CO_2 adsorbent and metallic catalyst, respectively. The addition of renewable H_2, allows DFM to convert the adsorbed CO_2 to CH_4 via Sabatier reaction.

The DFM function process includes two separate steps: CO_2 adsorption and methanation. The first adsorbs CO_2 from a power plant effluent, saturating the adsorbent. The CO_2 feed gas is then diverted to a second DFM parallel reactor for continuous capture. The CO_2-saturated DFM system is then fed renewable H_2 for methanation. The heat released from methanation drives the CO_2 to desorb from the alkaline sites (spillover) which diffuses to the catalytic sites for methanation. Under this concept, the DFM methane production is enhanced by the presence of the alkaline adsorbent. Continuous operation is achieved with a swing reactor system where one functions for CO_2 adsorption while the second for methanation with a switch upon saturation of CO_2 or completion of methanation.

The first generation DFM was developed with a composition of 5% Ru, 10% CaO / Al_2O_3 in the powder form. This combination of Ru and CaO was determined as the optimum composition

among other Ru to CaO ratio candidates with the largest CH_4 production (0.50 g-mol) per kg of DFM [17]. The feasibility and stability of it in air- and steam-containing CO_2 feed gas was also demonstrated [141].

The first generation DFM was prepared into tablet form and parametric studies conducted in simulated flue gas (O_2- and steam-containing) [141]. In this study, parameters of CO_2 adsorption (O_2 effect on Ru) time on stream (TOS), reaction temperature, extent of CO_2 adsorption and methanation feed gas flow rates were evaluated. The material preparation method utilized ruthenium chloride in place of ruthenium nitrosylnitrate allowing more uniform penetration into the Al_2O_3 tablets.

Other precious and base metal catalysts for CO_2 methanation were investigated, including Rh, Pt, Pd, Ni and Co [18]. As the result, Ru and Rh were identified as the most active candidates for DFM while Ru is more preferred based on price and activity, although Rh has higher resistance to oxidizing conditions occurring in the adsorption step.

To further improve the CO_2 adsorption capacity and subsequent CH_4 production, new CO_2 adsorbents were developed. Alkali metal and alkali earth metals were tested as candidates to replace the CaO [18]. Different loadings of K_2CO_3, Na_2CO_3 and MgO all supported on γ-Al_2O_3 were tested for their CO_2 adsorption capacity and reversibility for CO_2 desorption under CO_2 partial pressure swing. 10% Na_2CO_3 / γ-Al_2O_3 and 10% K_2CO_3 / γ-Al_2O_3 showed almost double CO_2 uptake compared to the initial CaO-DFM. Little improvement for CO_2 adsorption was observed when the adsorbent loadings were further increased. MgO / γ-Al_2O_3 shows less CO_2 adsorption than CaO / γ-Al_2O_3.

The second generation DFM was synthesized replacing the 5% CaO with 10% Na_2CO_3 (precursor loading) as the adsorbent. Preliminary TGA cyclic tests with the new DFM

demonstrated superior performance over the CaO system. Therefore, the new DFM is now composed of 5% Ru, 10% Na_2CO_3 (precursor loading, 6.1% "Na_2O" after hydrogenation) / γ-Al_2O_3 and is the second generation DFM technology. Its performance is the subject of the current thesis.

Chapter 3: Experimental Methodology

3.1 Material synthesis

3.1.1 Preparation of DFM Powder with $Ru(NO)(NO_3)_3$

The powder DFM samples were prepared via incipient wetness impregnation on a high surface area commercial γ-Al_2O_3. The ruthenium (III) nitrosylnitrate ($Ru(NO)(NO_3)_3$, Ru 31.3% min) was provided by Alfa Aesar, Tewksbury, MA, USA. The Na_2CO_3 (Sigma-Aldrich, St. Louis, MO, USA) was used as the precursor for "Na_2O". The γ-Al_2O_3 powder (BASF, SBA-150, Iselin, NJ, USA) was dried in air at 120 °C for 2 hours prior to any impregnations to remove moisture and other adsorbed volatile components. The Na_2CO_3 was first impregnated into the γ-Al_2O_3 powder followed by drying at 120 °C for 2 hours then calcined at 400 °C for 4 hours in air. Subsequent Ru salt deposition was completed with drying at 120 °C for 2 hours and calcination at 250 °C for 2 hours in air to decompose the $Ru(NO)(NO_3)_3$. Repeated impregnations were conducted to reach the designed loadings as required. Higher calcination temperatures in air for Ru were avoided to prevent formation of volatile RuO_x compounds [142, 143].

3.1.2 Preparation of DFM Tablets/Powder with $RuCl_3$

Tablet γ-Al_2O_3 (5 × 5 mm) was supplied by SASOL (TH100, Hamburg, Germany). The tablet samples were prepared via incipient wetness with precipitation method for Ru impregnation. $Ru(OH)_3$ was precipitated in the Al_2O_3, with addition of slight excess NaOH (Ru : OH = 1 : 4.5), from an aqueous solution of $RuCl_3$ (ruthenium (III) chloride hydrate, $RuCl_3 \bullet xH_2O$, 99.9% PGM basis, Ru 38% min, Alfa Aesar, Tewksbury, MA, USA). The $RuCl_3$ gave more uniform penetration into the tablets compared to $Ru(NO)(NO_3)_3$, therefore it was used as the precursor for all

impregnations of tablets. $RuCl_3$ was also used as the catalyst precursor for the impregnation of the Al_2O_3 (BASF) powder for the kinetic study.

A water wash was introduced after precipitation of water-insoluble $Ru(OH)_3$ to remove unwanted chloride followed by drying at 120 °C for 2 hours and calcination at 250 °C for 2 hours in air to decompose $Ru(OH)_3$ to RuO_x. An aqueous solution of (~ 20 wt%) Na_2CO_3 was used for producing the Na_2O in the tablets, with drying and calcination at 120 °C and 250 °C, respectively. The preparation process flow is shown in Figure 3.1.

Figure 3.1 DFM tablets preparation process flow using $RuCl_3$ as the Ru precursor. A slight excess of NaOH was used with a ratio of Ru:OH = 1:4.5 to precipitate $Ru(OH)_3$. Water wash and filtration was introduced to remove chloride. Drying and calcination steps were conducted in air.

3.2 Thermogravimetric Analysis (TGA) Tests

Thermogravimetric analyses were conducted in a SAT 449 F3 Jupiter NETZSCH unit, which is capable to precisely measure the sample mass change at programed temperatures and feed gases simultaneously. Either 50 mg or 20 mg of powder samples were loaded for the tests in an alumina crucible and secured in the instrument. The operational flow rates were at 40 ml/min and temperatures at 320 °C for the preliminary performance and stability tests. For the kinetic studies, the temperature ranged from 200 °C to 320 °C, while the feed gases and corresponding time

durations were varied. All samples were degassed in pure flowing nitrogen at designed temperatures. Stable materials were achieved as demonstrated by the absence of mass change in the TGA. Detailed programs for each test are indicated in the corresponding chapters.

3.3 Scaled-Up Fixed Bed Reactor

To scale up the DFM technology toward commercialization, it is necessary to use tableted DFM and thus a larger diameter reactor was built to contain larger amounts of sample. Cyclic tests of CO_2 adsorption from a simulated flue gas and catalytic conversion to methane were sequentially conducted in the reactor, shown in Figure 3.2, using 10 grams of 5 mm × 5 mm tableted DFM. Compressed gases (TechAir) were mixed at the designed flow rates controlled by mass flow controllers (MKS Instruments). Water was injected with a syringe pump (Cole-Parmer) and co mixed with the other gases into the reactor feed tube wrapped with heating tape to maintain at 125 °C. The DFM tablets were packed in a standard quartz tube (O.D. = 25 mm, I.D. = 20 mm, length = 570 mm) supported on an uncoated ceramic monolith in the proper temperature zone of the tube. Glass beads (D.I. of 6 mm, Fisher Scientific) filled the downstream dead volume to ensure rapid and improved analysis. A micro thermal furnace (MTSC12.5R-0.75X18-1Z-IOT, Mellen) was placed outside of the reactor tube with temperature feedback control by a thermocouple (K-type, Omega) at the inlet of the DFM bed. The product gas was chilled in an ice bath to remove H_2O from the feed or from that generated during methanation prior to entrance into the Enerac analyzer.

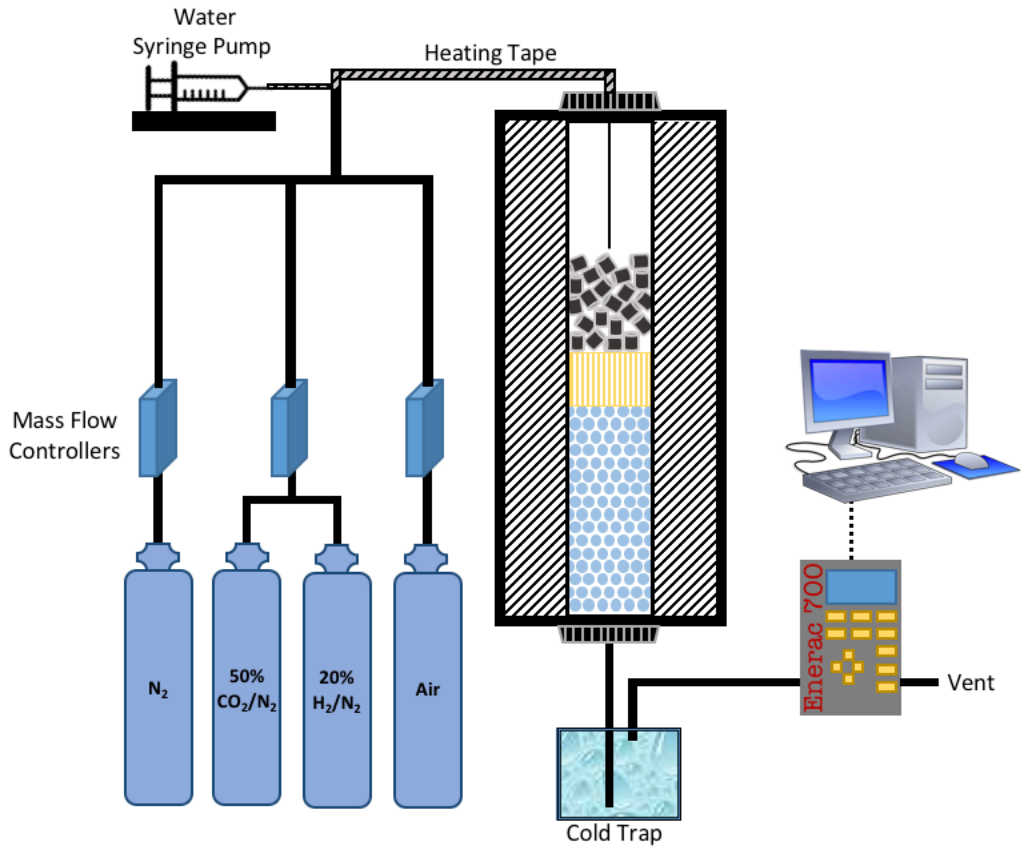

Figure 3.2 Diagram of scaled-up fixed bed reactor. The N_2 cylinder was used either exclusively or simultaneously with the 50% CO_2 / N_2 or the 20% H_2 / N_2 to dilute the CO_2 and H_2 to designed concentration. The three mass flow controllers are under command of a Multi-Channel Flow Ratio/Pressure Controller.

A calibrated Enerac Model 700 was connected to the ice-cooled exhaust gas of the fixed bed reactor equipped with nondispersive-infrared sensors (error within 3% of reading) which measured CO, CO_2 and CH_4 at a frequency of 1 Hz while the O_2 (error within 0.2% of reading) content was measured electrochemically also in the Enerac. The Enerac analyzer unit measures percentage or ppm of the components in the outlet gas allowing the calculation of the amount of CO_2 adsorbed, CO_2 desorbed, CH_4 generated and O_2 consumed based on their concentrations. Mass flow controllers were calibrated with a precisely calibrated bubble meter. The Enerac sensors

were calibrated using composition-known compressed gases for CO_2, CH_4 and O_2, and its accuracy were monitored via the same method.

3.4 Cyclic Tests on the Scale-up Fixed Bed Reactor

The scale-up fixed bed reactor contained 10 grams of tablet DFM comprised of 5% Ru, 6.1% "Na_2O" / Al_2O_3 (5 mm × 5 mm). Tests were performed for performance stability, the effect of O_2, parametric and cyclic aging studies. Fresh samples were used for most of the tests. The only exception was for the long term cyclic aging study where the sample was the same batch used in the parametric study. CO_2 adsorption was conducted either in O_2-free 7.5% CO_2 / N_2 (for preliminary stability studies) or in simulated flue gas (7.5% CO_2, 4.5% O_2, 15% H_2O vapor and balanced N_2, for more advanced studies). The methanation step was conducted in either 5% H_2 (for the preliminary O_2-containing stability study) or 15% H_2 / N_2 (for parametric and long term aging studies) at designed temperatures and flow rates. The program for each test is described in detail in the corresponding chapters.

3.5 Characterizations of Tablet DFM

3.5.1 BET Specific Surface Area and H_2 Chemisorption

BET specific surface area and H_2 chemisorption tests were performed using a ChemBET Pulsar TPR/TPD unit (Quantachrome) with crushed fresh and aged tablet DFM (into 6~8 pieces per tablet in the sample U-tube) after degassing. The fresh sample is defined as that prepared via the method mentioned in section 3.1.2, while the aged tablet DFM referred to the batch of sample that had undergone both the parametric study (chapter 7) and aging studies (section 8.1).

The internal surface area was measured from the standard single-point BET specific surface area method at 77 K cooled by liquid nitrogen. Ruthenium metal dispersion was obtained at room temperature via H_2 chemisorption after reduction in situ in 10% H_2 / N_2 at 320 °C and 30 ml/min for 21 h (fresh) and 1 h (aged). It was assumed that stoichiometry for chemisorption is one H atom per Ru site.

3.5.2 X-ray Diffraction (XRD)

X-ray diffraction (XRD) patterns of the ground fresh and aged DFM were performed using a PANalytical XPert3 Powder XRD. Patterns of bulk Na_2CO_3 and γ-Al_2O_3 powder were also scanned for comparison. The XRD is equipped with Cu K-α radiation, and the diffraction data was obtained at $2\theta = 5° \sim 80°$ with a step size of 0.10.

3.5.3 Transmission Electron Microscopy (TEM) and Energy-dispersive X-ray Spectroscopy (EDS)

The transmission electron microscopy (TEM) image and energy-dispersive X-ray spectroscopy (EDS) mapping was conducted by FEI Talos F200X TEM at 200 kV. The images were taken with the camera lens of 205 mm. The scanning transmission electron microscope (STEM) EDS mapping was obtained with the size of the selected Condenser 2 aperture at 50 μm and the spot size was 9. The EDS scans were acquired by Super X-EDS system. Four silicon drift detectors (SDD).

Chapter 4: Performance and Stability on powder DFM

The Ru, "Na_2O" DFM was developed based on improvements over the first generation material in which CaO was used as the adsorbent (Ru, CaO DFM). Replacing CaO with Na_2O (H_2 reduction from Al_2O_3 supported Na_2CO_3 precursor) resulted in much greater CO_2 capture capacity and subsequently enhanced methanation [18]. In order to be consistent with the first generation DFM, the new carbonate adsorbent was developed via the same preparation method of incipient wetness impregnation using $Ru(NO)(NO_3)_3$ as the catalyst precursor. In this chapter, the second generation DFM, in powder form, was evaluated in several TGA tests for its performance and stability.

4.1 Carbonate Hydrogenation with Ru present

Bulk Na_2CO_3 is known to be very stable at low and medium temperature with decomposition at 850 °C. The decomposition temperature of Na_2CO_3 to Na_2O and CO_2 was dramatically decreased from 850 °C to 135 °C when supported due to reaction of the carbonate with the γ-Al_2O_3 support [144]. To understand the role of Ru in the second generation DFM, comprising Ru and Na_2CO_3 on γ-Al_2O_3, a pre-treatment study was conducted in the presence of H_2. Since Ru was introduced in the form of ruthenium nitrosylnitrate, the sample had to be activated in a reductive H_2 atmosphere to form active metallic Ru sites which also hydrogenate the carbonate.

A TGA test was conducted with 50 mg of unsupported 1.44% Ru / Na_2CO_3 (with no high surface area support) prepared from $Ru(NO)(NO_3)_3$ precursor by impregnation via incipient wetness and calcined at 250 °C for 2 hours in air. A Low loading of Ru and the pre-calcination were used to decrease the extreme mass change due to the nitrate decomposition of the Ru salt and

any hydrogenation of the carbonate. The pre-conditioned sample, was loaded into the unit and exposed to a pure N_2 flow at 320 °C for an hour followed by 2% H_2/N_2 and then 5% CO_2/N_2 for 2 hours each. The test result is shown in Figure 4.1.

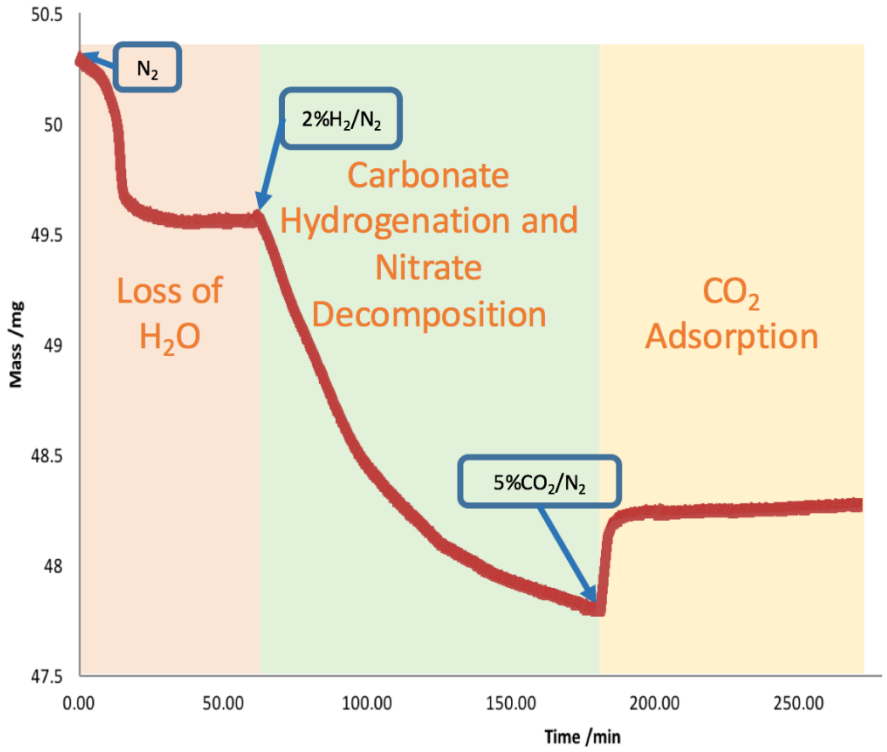

Figure 4.1 TGA result with 50 mg of 1.44% Ru / Na_2CO_3 powder operated at 320 ℃ in corresponding gaseous atmosphere at 40 ml/min.

From Figure 4.1, stable mass was obtained after degassing in pure N_2 at 320 °C. Ru nitrosylnitrate decomposition was expected during the H_2 activation (reduction) step, however, a greater weight loss was observed indicating hydrogenation of the carbonate had occurred. The total mass loss in this step was 1.763 mg. Assuming the $Ru(NO)(NO_3)_3$ remained in its original form as it is in the precursor at the H_2 introduction point, the expected mass loss due to nitrosylnitrate decomposition to gaseous products would be 1.332 mg or 65.37% of the total mass loss. Therefore,

the residual mass loss (an additional 34.63%) can be explained by carbonate hydrogenation catalyzed by the activated Ru metal. It is clear from Figure 4.1 that a continuing weight loss occurs beyond the two-hour exposure to H_2 atmosphere due to slow carbonate hydrogenation. The production of CH_4 as the product was later verified analytically in reactor tests.

After the H_2 treatment, the sample chemi-adsorbed CO_2 in the depleted carbonate sites. Since the material was unsupported and not dispersed, the CO_2 adsorption capacity was small due to fewer adsorption sites. The mass gained from CO_2 adsorption is greater than the theoretical maximum amount of CO_2 that can be adsorbed by the 1.44% Ru. The Ru itself catalyzed the hydrogenation of the bulk Na_2CO_3 at 320 °C. The solid product of hydrogenation is assumed to be Na_2O, which has a strong affinity for adsorbing CO_2.

The Ru catalyzed carbonate hydrogenation produces CH_4 along with what is assumed to be Na_2O although its exact composition has not been directly confirmed. It does however have a large affinity for CO_2 adsorption which is an important result for the DFM technology.

4.2 3-Cycle TGA Test for Stability of the DFM powder

The new DFM showed good CO_2 adsorption and methane production. What is even more critical for any materials is its performance stability in the application for which it is to be used. A preliminary stability test with three identical cycles of CO_2 adsorption and methanation was conducted on the new powder DFM with Ru as the catalyst.

50.5 mg of the new powder DFM using $Ru(NO)(NO_3)_3$ as the precursor was loaded in the TGA unit for a 3-cycle test at 320 °C with a flow rate of 40 ml/min for all gas feeds. The sample was pre-treated in 2% H_2 / N_2 for an hour to obtain active Ru metallic sites and to hydrogenate the carbonate to produce "Na_2O" sites. The sample was thoroughly reduced as demonstrated by the

absence of any additional mass change in TGA. Each cycle included three sections: 1) CO_2 adsorption in 5% CO_2 / N_2 for 30 min; 2) pure N_2 purge of the residual CO_2 in the reaction chamber for 30 min; 3) methanation in 2% H_2/ N_2 for 30 min. The test results are shown in Figure 4.2.

The first cycle has the highest CO_2 uptake capacity, due to depletion of the carbonate during the pretreatment generating the most available CO_2 adsorption sites. A slight mass loss was observed for every N_2 purge due to some reversible CO_2 desorption. The following hydrogenation of adsorbed CO_2 was demonstrated by the decreased mass but was not completely depleted within the 30-min H_2 exposure. This caused a decrease in CO_2 adsorption in the second and third cycle. It is also conceivable that some of the Ru sites (which adsorb CO_2 when reduced) may be partially oxidized by the dissociative adsorption of CO_2 to CO and O and thus will not adsorb CO_2 [140].

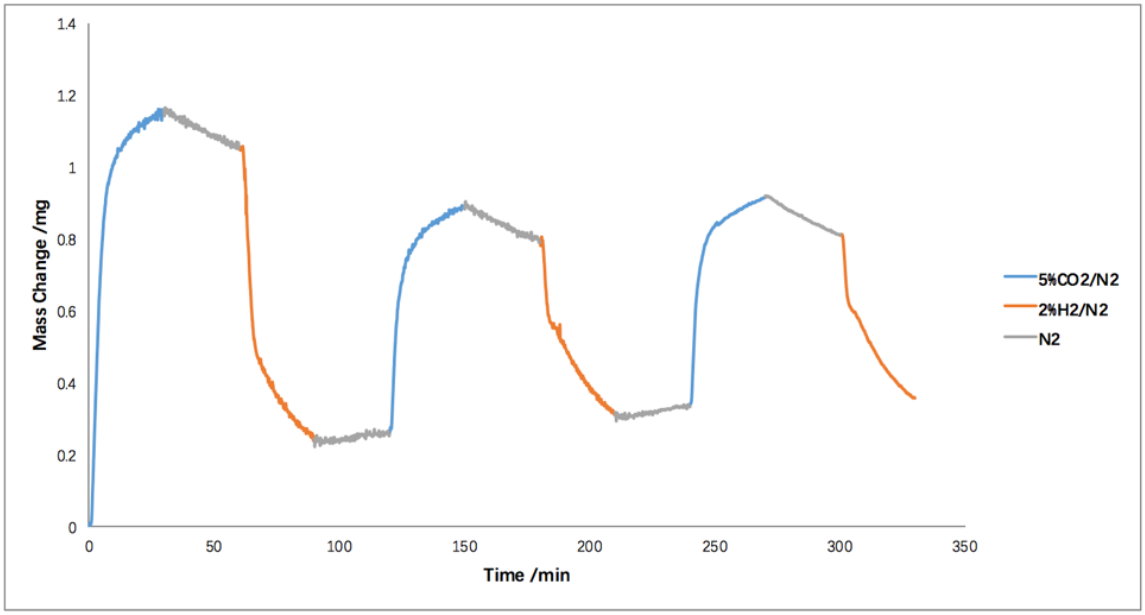

Figure 4.2 3-cycle TGA test for preliminary stability of the powder DFM. The blue lines indicate CO_2 adsorption in 5% CO_2 / N_2; grey lines indicate pure N_2 purge between adsorption and methanation, also between cycles; orange lines indicate methanation in 2% H_2 / N_2. 30 min for each section; 320 ℃; 40 ml/min.

Both of these arguments suggest that the 30-min exposure in 2% H_2 / N_2 was not sufficient to completely hydrogenate the adsorbed CO_2 and/or to reduce any oxides of Ru. This is also evident since the mass gained from adsorption didn't return to its initial state as in the start of the first cycle.

The amount of CO_2 adsorbed and desorbed in cycle 2 and 3 show consistent results indicating initial stability of the powder DFM. It was proposed that the decreased CO_2 adsorption capacities could be recovered by intensified H_2 exposure during the methanation step. The weight loss observed when 2% H_2 / N_2 is introduced in the three cycles shows first a rapid decrease followed by a slower one. It was speculated that the rate of methanation of the CO_2 adsorbed on the Ru sites was faster than the CO_2 adsorbed on the "Na_2O" sites and by increasing H_2 exposure both rates, but especially the chemisorbed CO_2 on the "Na_2O", could be further enhanced. Experiments with increased H_2 exposure time were then conducted (Section 4.3).

4.3 CO_2 Hydrogenation with Prolonged Hydrogen Exposure Time

The unreacted adsorbed CO_2 shown in Figure 4.2 is expected to be hydrogenated with intensified hydrogen exposure, including prolonged exposure time. Another 3-cycle TGA test was conducted with a new fresh sample of the powder DFM to test this hypothesis. Test conditions were similar to the 3-cycle test described in section 4.2 but with an overnight hydrogen exposure for the methanation step during cycle 1.

50 mg of 5% Ru, 6.1% "Na_2O" / Al_2O_3 powder DFM sample was subjected to a one-hour pretreatment in 2% H_2 / N_2 at 320 °C prior to adsorption of CO_2. Each cycle contains CO_2 adsorption and methanation steps with 30-min pure N_2 purge between cycles. CO_2 adsorption was conducted in 5% CO_2 / N_2 for 30 minutes for each cycle and methanation in 2% H_2 / N_2 for 10.5

hours (overnight) for the first cycle but only 30 minutes for the second and third methanation step. The test results are shown in Figure 4.3. During the pretreatment (not shown in the figure), 6 mg of mass loss was observed owing to hydrogenation of both nitrosylnitrate and carbonate with no additional loss.

Rapid uptake of CO_2 of 1.2 mg occurred in the adsorption step during the first cycle. Upon addition of 2% H_2 / N_2, three distinct slopes of weight loss were observed. The largest slope, lasted for about 5 min corresponding to a weight loss of 0.086 mg/min. The second, between roughly 5-40 min of the hydrogenation process, was 0.00952 mg/min and the third about 0.00195 mg/min. The first mass loss, associated with the largest slope, occurs from 1.2 mg to 0.66 mg is likely due to methanation of the CO_2 adsorbed on the metallic Ru sites. This weight loss is approximately 50% of the Ru atoms present assuming 1 CO_2 adsorbed on 1 Ru site. It is also possible that 1 CO_2 may adsorb on two Ru sites for dissociative adsorption to CO and atomic O [140]. The second slope has a weight loss of about 0.45 mg; speculated to be the hydrogenation of the weakly adsorbed CO_2 on the alkaline adsorbent. Here most of the released CO_2 has spilled over to the Ru sites. The weight loss associated with the lowest slope is less than 0.2 mg and is believed to be hydrogenation of the bulk carbonate that was reformed during CO_2 adsorption.

For the second cycle, the mass gain for CO_2 adsorption was similar to the first indicating more complete hydrogenation and thorough depletion of the adsorbed CO_2 and any O on Ru. However, with only 30 min of hydrogen exposure, the weight loss was significantly less demonstrating the importance of H_2 exposure time to complete hydrogenation. In the third cycle, with a 30-minute exposure time the CO_2 uptake was lower and similar to those shown in Figure 4.2.

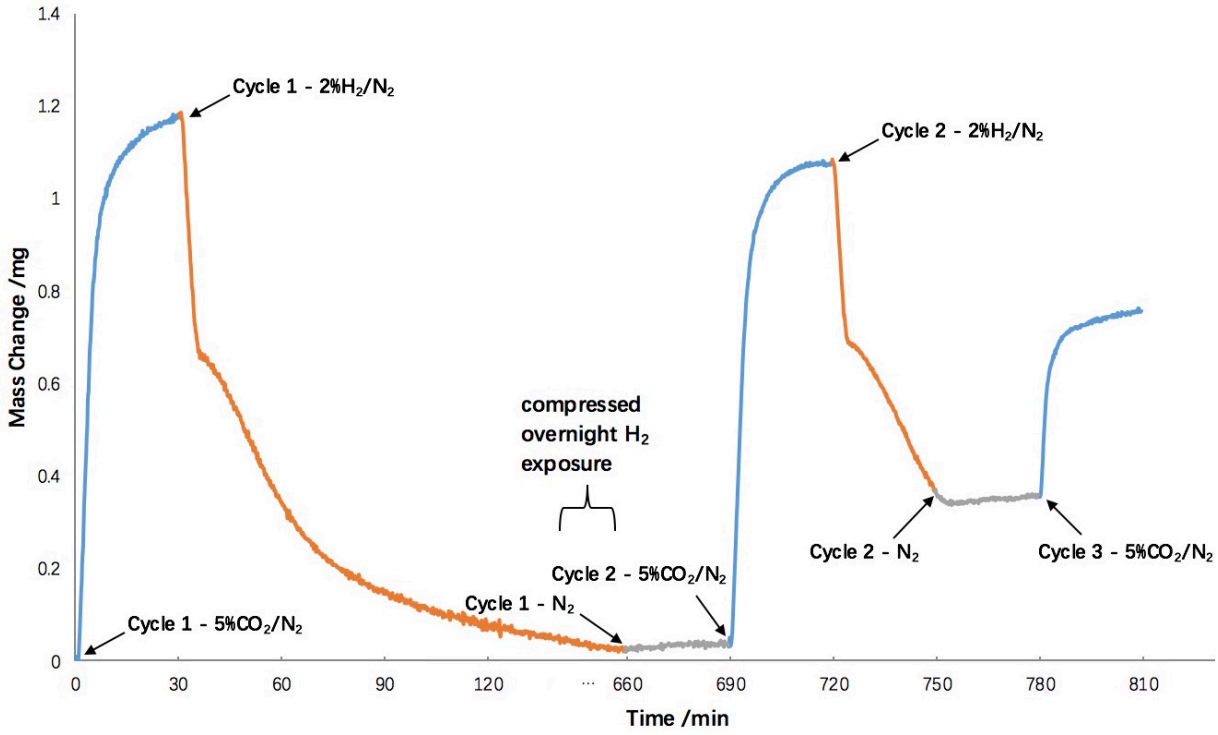

Figure 4.3 TGA result of the prolonged hydrogen exposure test for the powder DFM at 320 ℃. The plot excluded the pretreatment step in 2% H_2 / N_2. The long tail of low weight loss in the first cycle was compressed indicating an overnight (10.5 h) hydrogen exposure.

It is obvious that CO_2 uptake is dependent on the extent of the carbonate (both initial and reformed) and adsorbed CO_2 depletion which is impacted by hydrogen exposure time and could also by hydrogen partial pressure. In conclusion, thorough reduction in the hydrogen atmosphere is critical for the DFM to maintain its maximum capacity of CO_2 adsorption and subsequent methanation. This provided valuable data for more advanced studies indicated in subsequent chapters of this thesis.

Chapter 5: Short-Term Cyclic Tests on the Reactor with Tablet DFM

A commercial process for DFM will need to utilize tablets or particulate materials for a fixed bed application and thus it was necessary to scale up from current powdered material to particulate structures. For example, in a fixed bed reactor, powders have high pressure drop [145] and expose operators to possible risk of chronic human health issues such as respiratory diseases and lung cancer [146].

A preparation method was developed for producing 5 mm × 5 mm Al_2O_3 tablet supported DFM. A key requirement necessary was a uniform distribution of the Ru throughout the tablets to maximize contact with the uniformly distributed adsorbent. Current studies showed that the best results were obtained with γ-Al_2O_3 (SASOL, TH100) tablets and $RuCl_3$. An aqueous solution of $Ru(NO)(NO_3)_3$ did not penetrate uniformly into the depths of the tablets so it was eliminated from consideration. The impregnated $RuCl_3$ (which provided uniform penetration) was precipitated as $Ru(OH)_3$ (RuO_x after calcination) within the tablet using small amount of NaOH.

Short-term cyclic tests were conducted to verify the tablet DFM performance stability in O_2-containing simulated flue gas applications. This chapter contains two sets of cyclic tests (one without and a second with an O_2-containing simulated flue gas) for the tablet DFM.

5.1 Cyclic Stability Tests of Tablet DFM in O_2- and Steam-free Feeds

Ten grams of tablet DFM with a composition of 5% Ru, 6.1% "Na_2O" / Al_2O_3 was loaded in the fixed bed reactor and subjected to 10 cycles of adsorption and methanation at 320 °C and 300 ml/min (GHSV = 1432 h^{-1}) for total flow rates. The sequential operational steps are shown in Figure 5.1. A pre-reduction was used with 5% H_2 / N_2 to reduce RuO_x (obtained from preparation calcination in air) to active metallic Ru and to hydrogenate impregnated carbonate to "Na_2O".

Each cycle was composed of a CO_2 adsorption step in 7.5% CO_2 / N_2 for 30 min to reach CO_2 saturation followed by methanation using 5% H_2 / N_2 for 30 min. No N_2 purge was necessary since no O_2 was present.

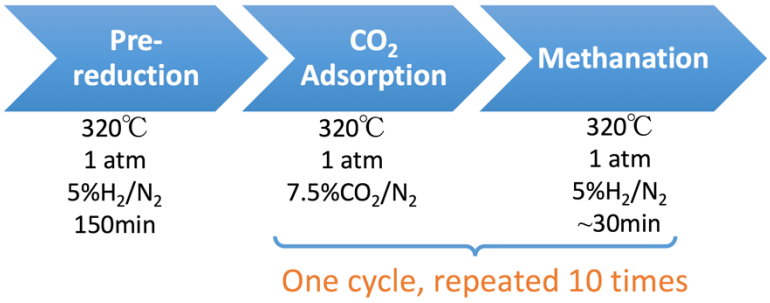

Figure 5.1 Sequential operational steps for the cyclic test on the tablet DFM in O_2- and steam-free CO_2 feed gas. 10 identical cycles of CO_2 adsorption and catalytic methanation were operated repeatedly at 320 ℃ and 300 ml/min.

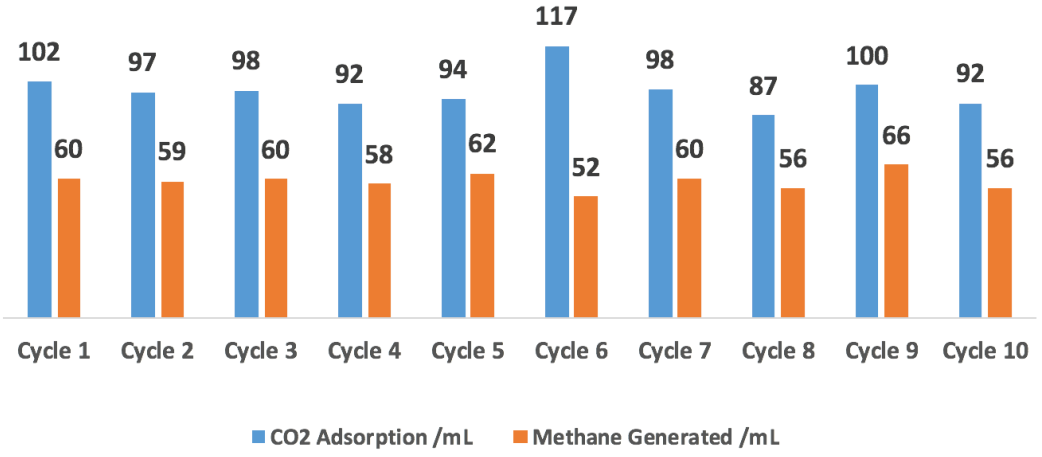

Figure 5.2 Ten identical cycles of CO_2 adsorption and methanation with 10 grams of fresh tablet DFM (5% Ru, 6.1% "Na_2O" / Al_2O_3) in the fixed bed reactor. Conditions: 150-min pre-reduction in 5% H_2 / N_2; 30-min 7.5% CO_2 / N_2 for CO_2 adsorption; 30-min 5% H_2 / N_2 for methanation; 320 ℃; 300 ml/min. The pre-reduction was introduced prior to the cycles (not shown).

Ten identical cycles of CO_2 adsorption (blue columns) and methanation (orange columns) were conducted and the results are shown in Figure 5.2. Given the slow kinetics for bulk carbonate hydrogenation as seen in Figure 4.3 at 2% H_2 / N_2, the H_2 was increased to 5% H_2 / N_2. The tablet DFM achieved stable adsorption and methanation performance for 10 successive cycles and is expected to maintain stability over additional cycles. However, the average conversion efficiency of the adsorbed CO_2 converted to methane was only 60.5%. A large amount of desorbed CO_2 was observed at the reactor outlet. The 39.5% unreacted CO_2 released is likely due to its premature desorption caused by the large exotherm of methanation. Therefore, it may be necessary in the final process design to locate a small load of supported Ru catalyst (without adsorbent) downstream to complete methanation of the unconverted CO_2. Conditions of our experiments were controlled to avoid CO formation that is observed at higher temperatures and space velocities [140].

Although the primary commercial target of our research is focused on O_2-containing flue gas from a power plant effluent, there are O_2-free applications such as fermentation, land fill and cement manufacturing effluents that might be worth considering for the future. High stability was indicated in this cyclic test on the tablet DFM in O_2- and steam-free feed gas applications.

5.2 Cyclic Stability Test of Tablet DFM in O_2-Containing Simulated Flue Gas

Capture and conversion of CO_2 from a flue gas generated in a natural gas power plant presents the challenges of O_2 and steam on DFM stability especially Ru which can be oxidized during CO_2 capture. A 12-cycle test with simulated flue gas was conducted in the fixed bed reactor.

Ten grams of a fresh sample of tablet DFM was subjected to a 150-min 5% H_2 / N_2 pre-reduction step to obtain active metallic Ru and "Na_2O" from supported Na_2CO_3. CO_2 adsorption was conducted in a simulated flue gas composed of 7.5% CO_2, 4.5% O_2, 15% H_2O and balanced

N_2 for 30 min. A 3-min pure N_2 purge between CO_2 adsorption and the methanation step (and the reverse) was included to avoid explosive contact of H_2 and O_2. The twelve cycles were operated with 30-min methanation in 5% H_2 / N_2 after CO_2 adsorption and the N_2 purge step. Prior to the last two cycles a prolonged H_2 exposure was necessary to sustain performance. The 11th cycle was treated for extra 150 min with 5% H_2 / N_2 and the 12th cycle for 48 hours. It was speculated that the prolonged H_2 exposure was needed to reduce and regenerate the oxidized ruthenium from the adsorption step because of O_2 presence. The reaction temperature was 320 °C at a total flow rate of 300 ml/min. See Figure 5.3 for the 12-cycle process steps and Figure 5.4 for the results.

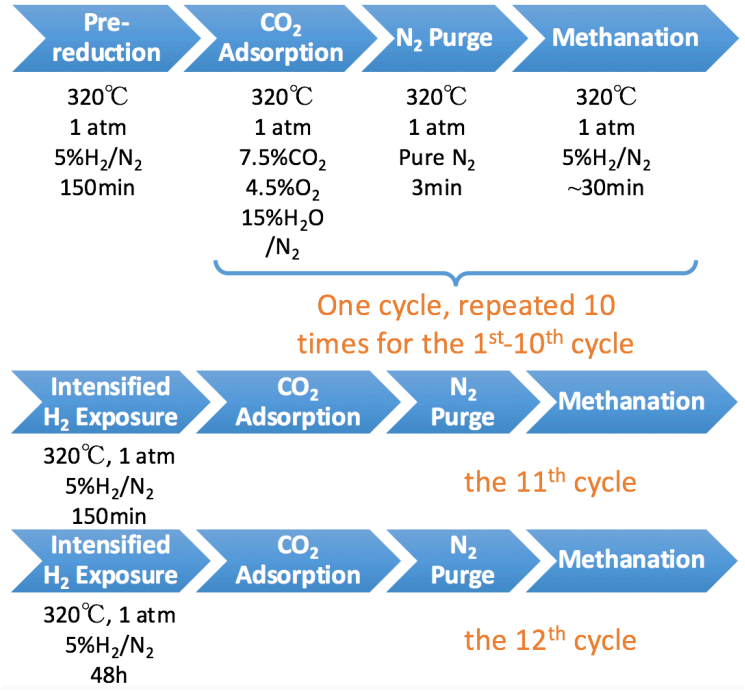

Figure 5.3 Process flow for the 12-cycle test operated in the fixed bed reactor. All of the cycles were continuously and identically operated for 30-min CO_2 adsorption in the simulated flue gas and 30-min methanation in 5% H_2 / N_2, but prior to the 11th and the 12th cycle prolonged H_2 exposure time was introduced with 150min and 48 h respectively.

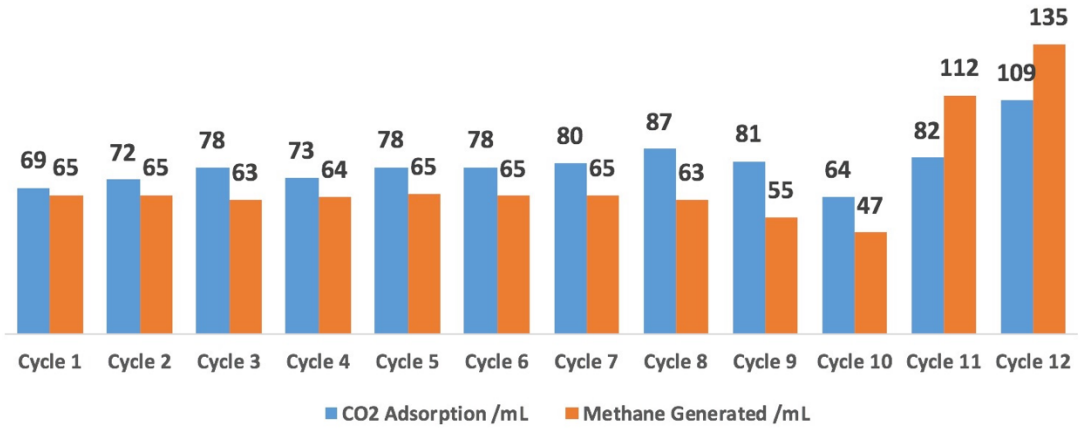

Figure 5.4 12-cycle test of 10 grams of tablet DFM in the fixed bed reactor. Conditions: 150-min pre-reduction in 5% H_2 /N_2 before the cycles; CO_2 adsorption in simulated flue gas for 30 min; methanation in 5% H_2 / N_2 for 30 min; prolonged H_2 exposure prior to the 11th cycle 150 min and the 12th for 48 h; 320 ℃; 300 ml/min.

Stable performance for both CO_2 adsorption and methanation were observed from the 1st to the 8th cycle, however deactivation began to appear in the 9th. This apparent deactivation was not observed in the O_2-free cyclic test as shown in Figure 5.2. Due to the presence of O_2 in the simulated flue gas, it was theorized that Ru was oxidized to inactive RuO_x resulting in a decrease of reduced active sites for both CO_2 adsorption and methanation. The 30-min exposure in 5% H_2 / N_2 during the first ten cycles was not sufficient to reduce the oxidized Ru, causing a loss in both adsorption and methanation performance. Before the 11th cycle, the material was subjected to an extra 150-min of hydrogen exposure, which recovered both the CO_2 adsorption and methanation performance. When the extra exposure to hydrogen was extended to 48 hours before the 12th cycle, both the capacities reached even higher levels. This again demonstrated the importance of H_2 partial pressure in maintaining Ru reduced while enhancing the rate of bulk carbonate hydrogenation.

It is noted that the amount of methane generated in the 11th and the 12th cycle was more than the CO_2 adsorbed in these two cycles respectively. It is speculated that the unconverted adsorbed CO_2 from the previous cycles (1st – 10th) accumulated in the sample and the prolonged H_2 exposure hydrogenated this part of carbonate and generated additional methane.

The average conversion of adsorbed CO_2 converted to methane during the 12-cycle test was 89.6%, which is a great improvement compare to the 10-cycle test in the dry CO_2 feed (60.5%). Though the overall CO_2 adsorption of the 12-cycle test in simulated flue gas was lower than the 10-cycle test in O_2-free CO_2 feed, the higher conversion efficiency is preferred. It is also conceivable that during methanation the water generated may have partially oxidized the surface of Ru. Therefore, a minimum H_2 partial pressure is required to maintain Ru in the reduced and active state. H_2 exposure intensity has been found as a critical parameter necessary for reducing the RuO_x formed during CO_2 adsorption and allowing methanation to proceed.

5.3 H_2 Partial Pressure Impact on Adsorbed CO_2 Methanation and RuO_x Reduction

As observed in Figure 5.4, the loss in performance was reversed by extending the exposure time of the DFM to the H_2 atmosphere. It is reasonable to assume that increasing the partial pressure of H_2 would have the same effect of maintaining Ru in the metallic and active state while increasing the extent of carbonate hydrogenation. This was demonstrated in Figure 5.5 where 10% H_2 / N_2 dramatically increased the amount of methane produced (131 ml) compared to 5% H_2 / N_2 (58.7 ml). This also points to the importance of the redox chemistry of Ru/RuO_x. It is logical to assume that during the 12-cycle simulated flue gas test (Figure 5.4), Ru was oxidized and there was insufficient H_2 to re-reduce it.

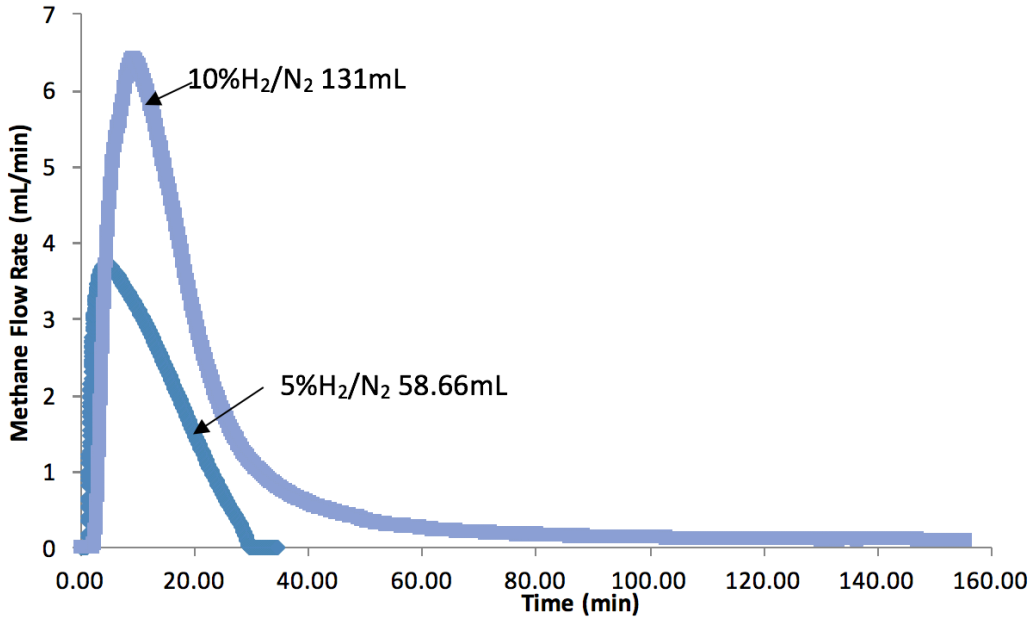

Figure 5.5 Methane production comparison of 5% H_2 /N_2 to 10% H_2 / N_2. The test was operated using 10 grams of 5% Ru, 10% Na_2CO_3 / Al_2O_3 tablets in the fixed bed reactor. The operational conditions were at 320 ℃, 300 ml/min of 7.5% CO_2 / N_2 for CO_2 adsorption. The volume of methane produced are shown.

The rate and extent of RuO_x reduction is critical for the flue gas operation so it was tested in TGA experiments to verify the hypothesis of the H_2 impact on RuO_x reduction. Results are shown in Figure 5.6. It is clear that the reduction rate (slope) increases with H_2 content (0.069 mg/min at 1.30% H_2 to 0.370 mg/min at 2.86% H_2). The most dramatic increase occurs for H_2 partial pressure > 1.3%. Equally as significant is the decrease in time for initiation of reduction as the H_2 content increases. This points to the reducibility of RuO_x to Ru, making it more suitable for the DFM flue gas processes relative to NiO_x to Ni metal [147] that requires temperatures in excess of 500 °C for reduction. A feed of 15% H_2 / N_2 was determined as the minimum operational H_2 content to maintain metallic active Ru sites and for rapid methanation of the surface carbonate.

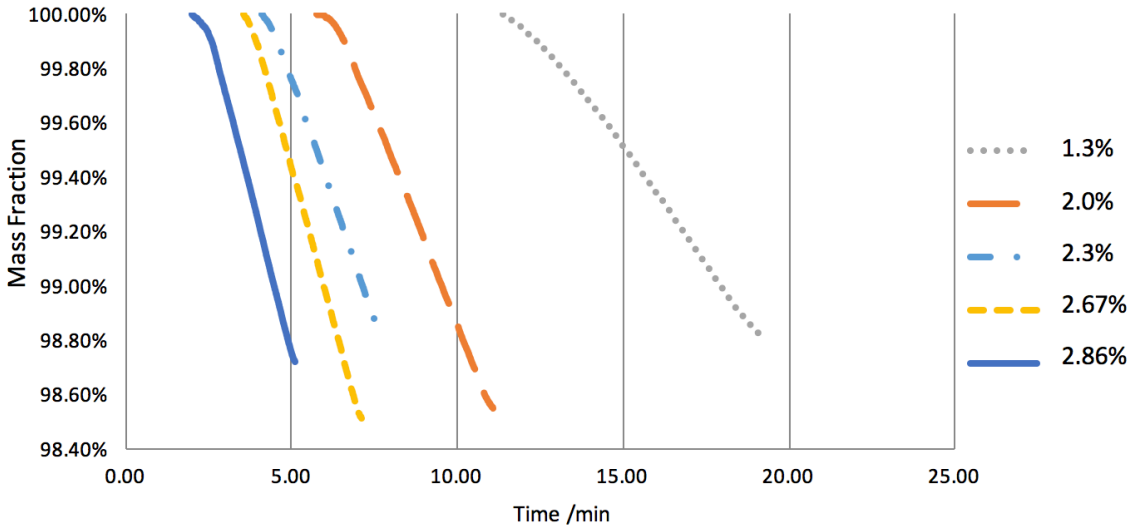

Figure 5.6 TGA results of RuO_x reduction on 50 mg air-oxidized 5% Ru / Al_2O_3 powder samples H_2 partial pressures from 1.3% to 2.86% at 300 ℃. Only reduction sections are shown.

5.4 Speculated Functional Pathway of the New DFM

The speculated pathways for each step and component in DFM are summarized in Table 5.1. The RuO_x, as prepared, must be activated to its active metallic state for methanation. For feeds containing O_2 it will be oxidized and lose its ability to adsorb CO_2. However, during methanation it will be re-reduced and re-activated for methane production. For O_2-free feed gas, Ru is both active for CO_2 adsorption and methanation.

For the new DFM, bulk carbonate hydrogenation occurs during pretreatment, producing Na_2O (NaOH with presence of H_2O) and CH_4 with CO_2 spill-over to Ru sites. Upon exposure to CO_2, it is reformed to a bulk carbonate species from CO_2 adsorption. The slowest step is the hydrogenation of the reformed bulk carbonate.

Table 5.1 Speculated function pathway of Ru and Na_2CO_3 in the new DFM.

Section	Ru Pathway	Na_2CO_3 Pathway
Pretreatment	$RuO_x + xH_2 \rightarrow Ru + xH_2O$	$Na_2CO_3 + 4\,H_2 \xrightarrow{Ru} "Na_2O" + CH_4 + 2H_2O$
O_2-free CO_2 feed	$Ru + CO_2 \longrightarrow Ru \cdots CO_2$	$"Na_2O" + \ CO_2 \longrightarrow "Na_2O" \cdots CO_2$
O_2-contain CO_2 feed	$Ru + \frac{x}{2}O_2 \longrightarrow RuO_x$	$"Na_2O" + \ CO_2 \longrightarrow "Na_2O" \cdots CO_2$
Methanation & hydrogenation	$RuO_x + xH_2 \rightarrow Ru + xH_2O$	$"Na_2O" \cdots CO_2 + 4\,H_2 \xrightarrow{Ru} "Na_2O" + CH_4 + H_2O$

Chapter 6: Empirical Rate Law for Adsorbed CO_2 Methanation

The rate of methanation in the DFM process is complicated by the two-step nature (endothermic desorption/spill over coupled to exothermic methanation) and the limited amount of adsorbed CO_2. Therefore, reactant order dependence cannot be achieved using typical kinetics. We approached this issue by hydrogenating the adsorbed CO_2 as a function of H_2 partial pressure and temperature and monitored the slope of the weight change vs. time using thermal gravimetric analysis (TGA). An empirical rate law of the adsorbed CO_2 methanation process is presented in the conclusion of this chapter.

6.1 Experimental

The kinetic study (using DFM powder to avoid mass transfer effects) of the adsorbed CO_2 methanation process was conducted using the TGA unit from which the mass change during methanation of the adsorbed CO_2 was recorded, and the rates of methanation reflected from the slope of the mass decrease. It was determined from reactor studies only methanation occur and thus the weight loss was due exclusively to methanation of adsorbed CO_2 and not the release from desorption. The 20 mg of powdered DFM sample was prepared via precipitation of $RuCl_3$, to $Ru(OH)_3$, by addition of small amount of NaOH into the impregnated Al_2O_3. The aqueous Na_2CO_3 solution was subsequently added to the DFM and reduced. The experimental conditions are stated in the corresponding figures.

All samples were pre-treated in 10% H_2 / N_2 at 320 °C for 90 minutes to obtain metallic Ru sites and to hydrogenate the impregnated carbonate to active CO_2 adsorption sites. The DFM was then exposed to 5% CO_2 / N_2 for CO_2 adsorption at the same temperature followed by a 2-hour exposure to the H_2 atmosphere. The methanation temperature was cooled from 320 °C to the

desired value (between 200 ~ 300 °C) in order to study the temperature dependence of CO_2 methanation.

6.2 H_2 Partial Pressure Dependence

The H_2 partial pressures were 17.9%, 15%, 10.3%, 5.1% and 2.5% obtained by dilution of a compressed 20.5% H_2 / N_2 gas in pure N_2. Batches of fresh 20 mg of the powder DFM were loaded in the TGA, pre-treated and CO_2 adsorption conducted before being hydrogenated at the specified H_2 partial pressure. TGA profiles for the different H_2 partial pressure are shown in Figure 6.1 and natural logarithm of the methanation rates vs. H_2 partial pressure in Figure 6.2.

The profile indicated the reaction being pseudo zero order above 15% H_2 but at lower H_2 values the slope decreases with H_2 partial pressure from which the apparent reaction order was calculated. Thus, the methanation rates (slopes) increases with H_2 partial pressure. The reaction order for H_2 was estimated from the slope of a plot of the natural logarithm of rate [ln (mass change/time)] vs. ln (H_2 partial pressure) (Figure 6.2) within the conversion ranges indicated by the asterisk. The data ranges selected are indicated by the asterisk mark in Figure 6.1 which were specified for each H_2 partial pressure condition. Rates were calculated from slope of the mass decrease vs. time at the maximum conversion CO_2 conversion. The apparent reaction order was 0.73.

The mass decrease in the TGA profile shows three sections. The first slow decrease (0~5 min) is believed due to the H_2 concentration building up in the TGA chamber in a protective N_2 gas. The last shallow part (beyond the asterisk-indicate range) was clearly attributed to the depletion of adsorbed CO_2 and was not used for the reaction order calculation.

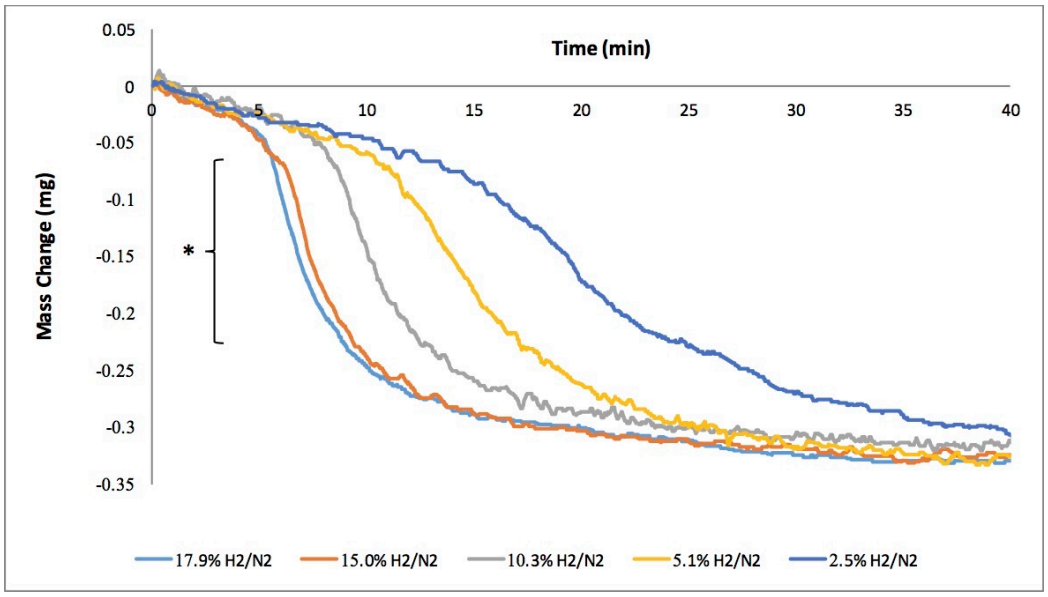

Figure 6.1 TGA profile for empirical rate law development related to the calculation of reaction orders for H_2 partial pressure. The asterisk shows the range from which the corresponding methanation rates were calculated. Test conditions: 20 mg of the powder DFM; pre-treated in 10% H_2 / N_2 for 90 min; CO_2 adsorption in 5% CO_2 / N_2 for 1 h; methanation in different H_2 partial pressure for 1 h; 320 ℃; 1 atm.

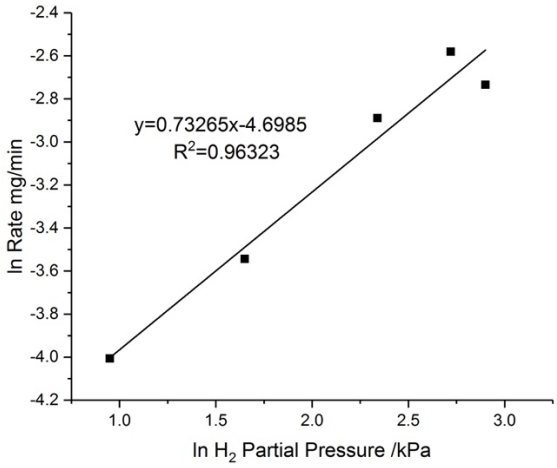

Figure 6.2 Natural logarithm of methanation rates vs. H_2 partial pressure for the empirical rate law.

6.3 CO_2 Coverage Dependence

20 mg of the powder DFM was tested in the TGA unit for the dependence of CO_2 coverage on the CO_2 methanation rate in 10% H_2 / N_2. CO_2 coverage (amount remaining on the surface) were 70%, 65%, 60% and 55% relative to monolayer/maximum CO_2 adsorption. The data range selected represents the highest rate of methanation for adsorbed CO_2. Typical TGA profiles and natural logarithm of methanation rates vs. natural logarithm of remaining CO_2 adsorbed graph are shown in Figure 6.3 and 6.4 respectively.

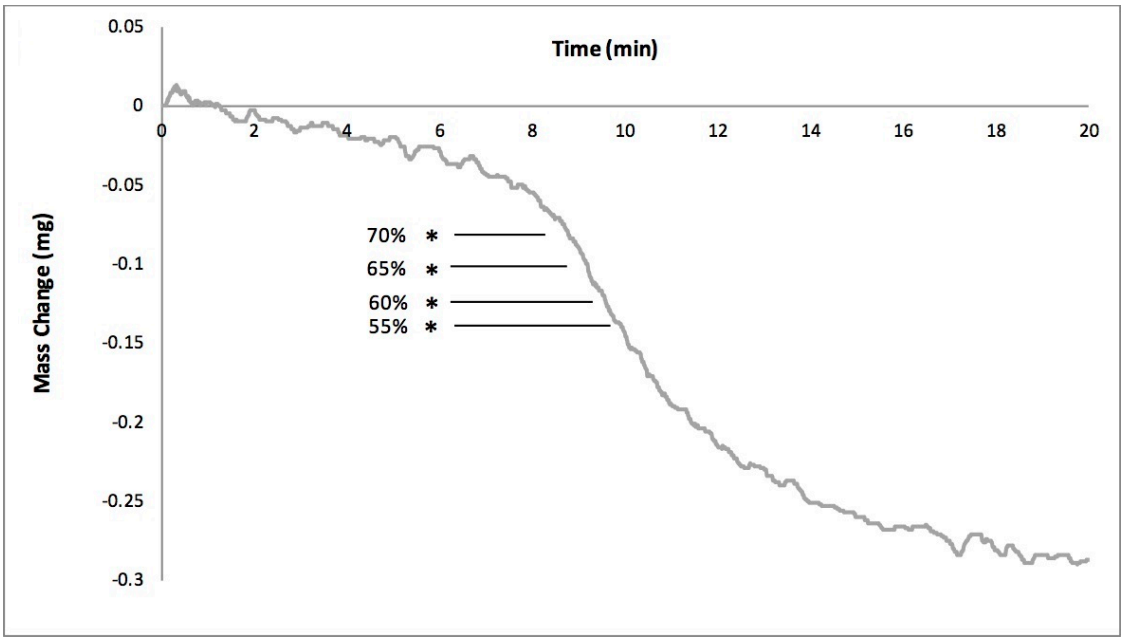

Figure 6.3 TGA profile for empirical rate law development related to the calculation of reaction orders for CO_2 coverage. The asterisk represents the specific data points used for initial methanation rates. Test conditions: 20 mg of the powder DFM; pre-treated in 10% H_2 / N_2 for 90 min; CO_2 adsorption in 5% CO_2 / N_2 for 1 h; methanation in 10% H_2 / N_2; 320 ℃; 1 atm.

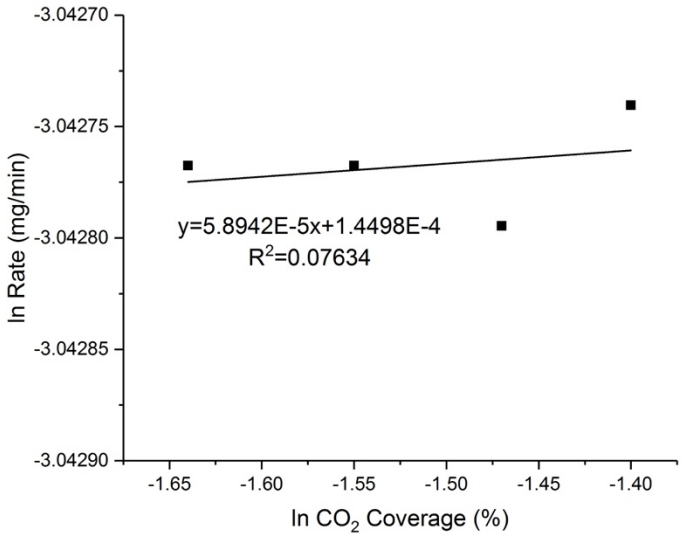

Figure 6.4 Natural logarithm of methanation rates vs. remained CO_2 adsorbed for the empirical rate law.

The slope of weight loss (methanation rate) vs. time (Figure 6.4) is essentially independent of the amount of CO_2 remaining on the surface where the rate yields maximum conversion . This is indicative of little or no rate dependence on adsorbed CO_2. The nearly zero value of R^2 also proves that no linear relationship exists between ln (rate) and ln (CO_2 coverage). Naturally, as the coverage decreases below about 25%, the rate is "starved" of CO_2 and some rate dependence must occur.

6.4 Temperature Dependence

CO_2 methanation was conducted at 200 °C, 250 °C, 280 °C, 300°C and 320°C to derive the empirical rate law of the methanation process. Fresh batches of 20 mg powder DFM were tested after pre-treatment and CO_2 adsorption at 320 °C followed by cooling to the designed temperatures for methanation in 10% H_2 / N_2. Figure 6.5 and 6.6 show the profile and natural logarithm of methanation rates vs. reciprocal of temperature.

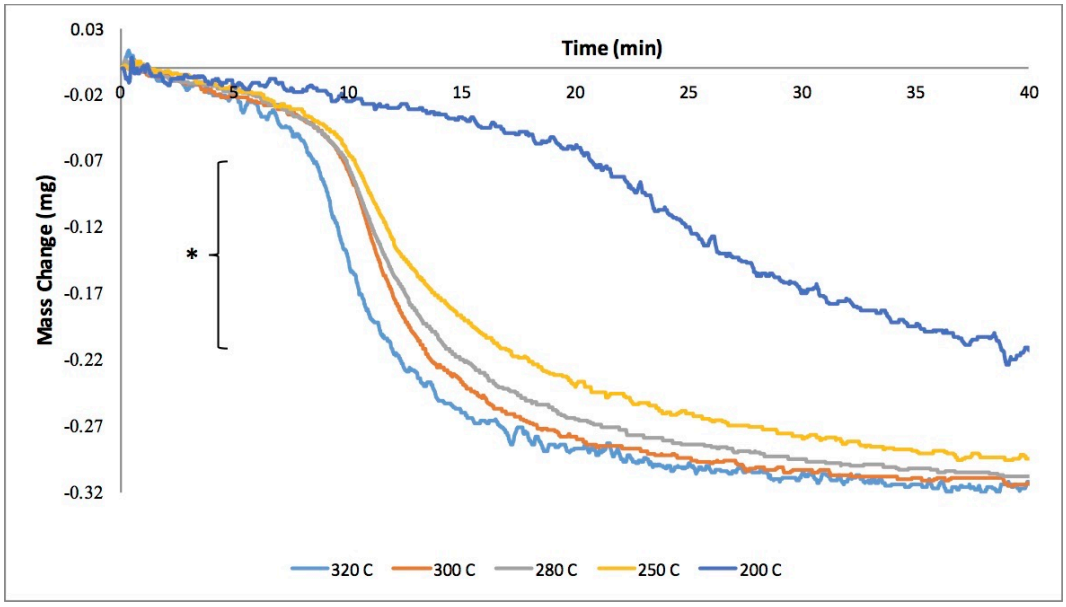

Figure 6.5 TGA profile for empirical rate law development for the apparent activation energy calculation. The asterisk shows the range for the temperature sensitivity (apparent activation energy) calculation. Test conditions: 20 mg of the powder DFM; pre-treated in 10% H_2 / N_2 for 90 min at 320 ℃; CO_2 adsorption in 5% CO_2 / N_2 for 1 h at 320 ℃; methanation in 10% H_2 / N_2 for 1 h at the designed temperatures; 1 atm.

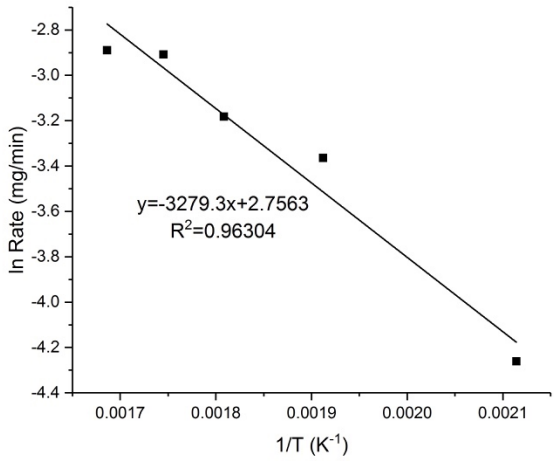

Figure 6.6 Natural logarithm of methanation rates vs. reciprocal of temperature for the empirical rate law.

The Arrhenius coefficient and apparent activation energy were measured between 200 °C and 320 °C. The Arrhenius coefficient was calculated from the y-intercept of Figure 6.6 and determined to be 89.92 m^{-1} $(H_2\ atm)^{-1}$. The apparent activation energy for the methanation process was derived from the slope of the linear relation line between 1/T and ln (rate) and was equal to 27.26 kJ/mon. Equation 6.1 and 6.2 shows the calculation of Arrhenius coefficient and apparent activation energy.

Arrhenius coefficient:

$$Intercept = lnA + 0.73265 \ln[H_2] + 5.8942 \times 10^{-5} ln[adsorbed\ CO_2]$$

$$A = 89.92\ min^{-1}\ (H_2\ atm^{-1}) \qquad \text{(Equation 6.1)}$$

Activation energy:

$$E_a = -slope \times R = -(-3279.3 \times R) = 3279.3 \times 8.314 = 27264.1 J/mol$$

(Equation 6.2)

6.5 Empirical Rate Law of Methanation Process

The empirical rate law is derived based on the above conclusions, see Equation 6.3. H_2 gas at the designed partial pressure was fed continuously sweeping away products of CH_4 and H_2O thereby avoiding equilibrium limitations. The activation energy for the methanation portion of the DFM is about ½ that reported in [131] by Duyar et al. for methanation of CO_2 by Ru / Al_2O_3. We speculate the methanation step of the DFM technology is limited by both kinetic and diffusion of desorbed CO_2 from "Na_2O" to the Ru metallic sites. Therefore, the activation energy reflects some diffusion limitation.

This empirical rate law highlights the positive influence of H_2 partial pressure on the DFM methanation process with virtually no dependence on adsorbed CO_2. Thus, the reaction orders are consistent with previous results for CO_2 methanation on Ru/Al_2O_3 [131] and the conclusion of short-term cyclic tests on the new DFM.

$$Rate\ of\ CH_4\ Formation = 89.92 \times e^{-\frac{27.26}{RT}} \times {p_{H_2}}^{0.73} \times [CO_2\ coverage]^{5.89\times10^{-5}}$$

(Equation 6.3)

$$in\ which, A = 89.92\ min^{-1}\ (H_2\ atm^{-1})$$

$$Ea = 27.26\ kJ/mol$$

$$Rate\ of\ CH_4\ formation\ in\ the\ unit\ of\ \frac{mg}{min};\ \ in\ kPa;\ [CO_2\ coverage] in\ mg.$$

Rate of CH_4 formation in the unit of mg/min; p_{H_2} in kPa; CO_2 coverage in percentage and represents the highest rate of CO_2 conversion from the selected 55%~70% range.

Chapter 7: Parametric Study on the Tablet DFM

The CO_2 capture (step 1) and conversion to methane (step 2) process for the DFM technology is more complex than a typical catalytic conversion due to its two-step nature. Its application to simulated flue gas with O_2 and steam present adds to the complexity. Process parameters, such as gas hourly space velocity (GHSV), temperature, linear velocity, DFM physical shape, etc. will have an impact on the commercial performance of DFM.

In this chapter, GHSV, temperature, impact of O_2 on Ru during the adsorption step and H_2 partial pressure were identified as primary process variables for subsequent aging studies. The parameter of exposure time is unique for application in O_2-containing flue gas because it relates to the extent of Ru oxidation and the initiation time of methane production.

7.1 Experimental

Ten grams of the tablet DFM sample (5 mm × 5 mm) was loaded into the fixed bed reactor in simulated flue gas for CO_2 capture and catalytic conversion. The Al_2O_3 supported sample was pretreated with 5% H_2 / N_2 at a GHSV of 1042 h^{-1} for 150 min at 320 °C to reduce and obtain active Ru metallic sites and to hydrogenate the precursor Na_2CO_3 to "Na_2O". The parameters studied were flow rate (GHSV) of all the gas feeds, temperature and flue gas exposure time (O_2 impact on Ru). H_2 partial pressure was fixed at 15% in N_2 based on that required to maintain Ru in a reduced state after its oxidation in the capture step. All other conditions were fixed. The variables studies are presented in the figures.

Each test cycle included 1) CO_2 adsorption in simulated flue gas at various flow rates and temperatures for different durations, 2) A 3-min N_2 purge and 3) methanation at varying flow rates with 15% H_2 / N_2. The simulated natural gas fired power plant flue gas feed consists of 7.5% CO_2,

4.5% O_2, 15% H_2O and balance N_2. The 3-min N_2 purge was needed between CO_2 adsorption and methanation to avoid contact of O_2 in the flue gas and H_2 for methanation to insure safety.

7.2 Simulated Flue Gas Flow Rate Effect

Results from the parametric study for the simulated flue gas flow rate effect are displayed in Figure 7.1. Captured CO_2 (yellow dots), desorbed CO_2 during 3-min N_2 purge (blue columns), CO_2 desorbed or unreacted during the methanation step (orange columns) and methane generated (grey columns) were quantified in gaseous volumes corrected to 20 °C in unit of ml.

For Figure 7.1 CO_2 adsorption (from simulated flue gas) was completed after about 30 minutes which is sufficient for the DFM to reach its maximum CO_2 capture capacity. A relatively stable amount of CO_2 uptake was observed with little influence from feed flow rates. After the N_2 purge, 15% H_2 / N_2 was fed at the same flow rate as the CO_2 feed, and methane produced was recorded until its value fell below 1000 ppm. Methanation and desorbed CO_2, both during 3-min N_2 purge and methanation, was relatively stable over all flow rates. The carbon balance was calculated from the sum of CH_4 produced and CO_2 desorbed relative CO_2 adsorbed from Figure 7.1 and was, from left to right, 99.01%, 100.59%, 97.60% and 100.36%.

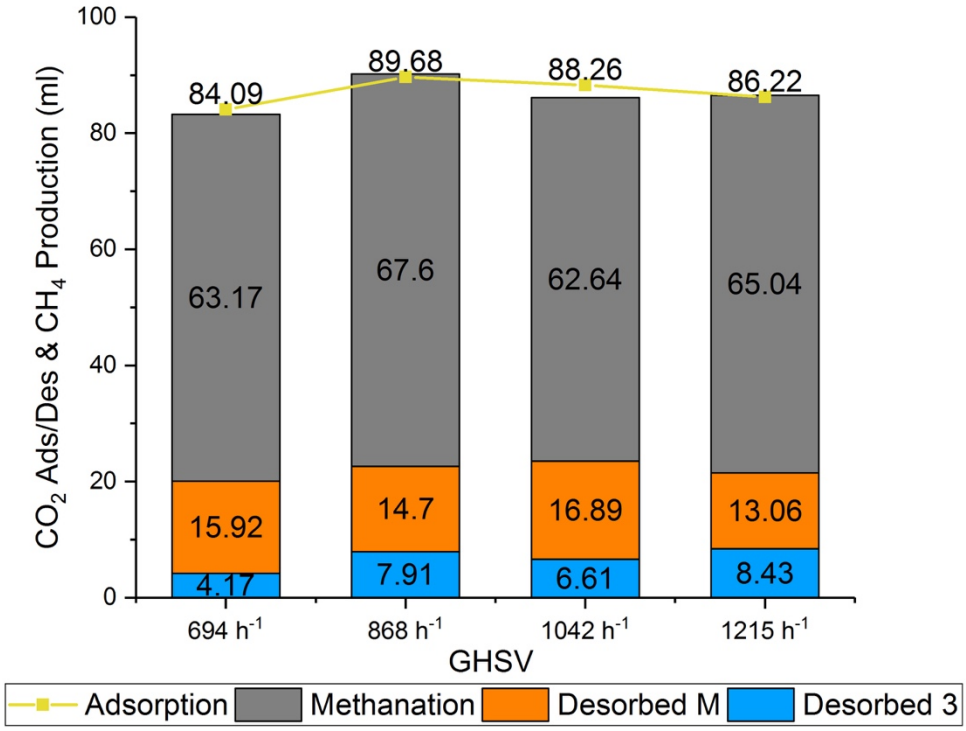

Figure 7.1 Parametric results (1 atm.) with simulated flue gas for 10 g of tablet DFM in the fixed bed reactor of the CO_2 adsorbed, CO_2 desorbed and methane generated in various feed gas flow rates at 320 ℃. Nomenclature: Desorption 3 = CO_2 desorbed during the 3-min N_2 purge; Desorption M = CO_2 desorbed during methanation. Methanation was always in 15% H_2 / N_2.

Figure 7.2 and Table 7.2 show the increased feed gas flow rates have little impact on the amount of CO_2 adsorbed and CH_4 generated. It did, however, enhance the rates of both as indicated by their slopes, and decreased completion time. In Figure 7.2 (A), fast CO_2 uptake rates were maintained at higher flow rates and reached similar uptake capacities. Similarly, for the rate of CH_4 production, see Figure 7.2 (B).

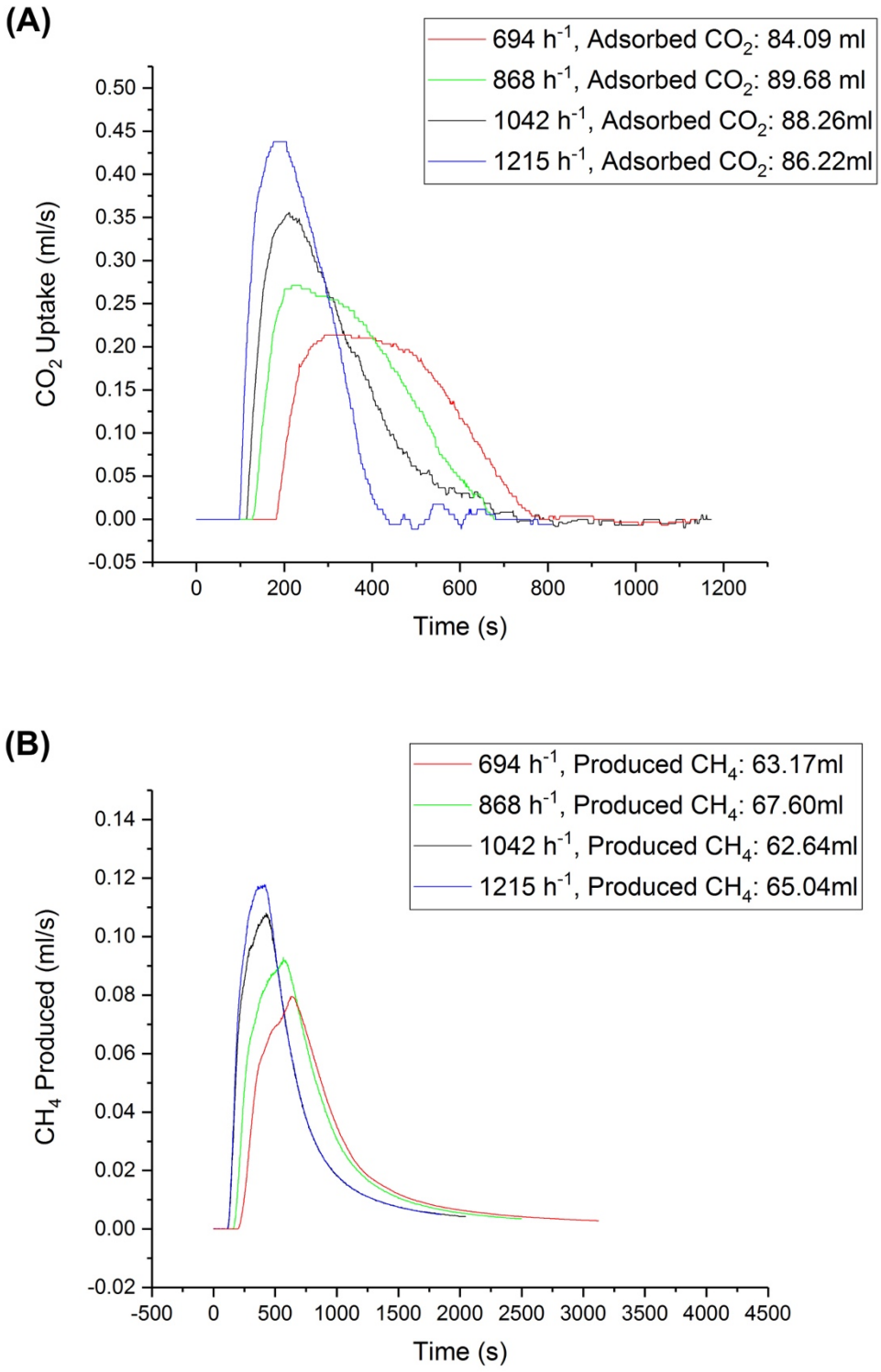

Figure 7.2 CO_2 adsorbed in simulated flue gas (A) and CH_4 produced in 15% H_2 / N_2 (B) vs. time at the flow rates indicated. Time origin points indicate the moment of gas changing. This data was used to generate Figure 7.1.

Both data records started at the beginning of each gas changing operation. Different breakthrough times showed in these two figures were mostly due to gas delivery delay to the DFM because of the different flow rates rather than indicating initiation delay of CO_2 adsorption and methanation. Table 7.2 shows millimoles of CO_2 adsorbed relative to millimoles of Na_2O present. Varying the space velocity or adsorption duration time is expected to impact the Ru oxidation reaction. This will be further addressed in section 7.4. The dispersion data indicates essentially one CO_2 molecule adsorbed for every 3 sites of Na_2O present.

Table 7.1 CO_2 uptake at different flow rates for the parametric study in the units of mmol.

GHSV	**694 h^{-1}**	**868 h^{-1}**	**1042 h^{-1}**	**1215 h^{-1}**
CO_2 Uptake (mmol)	3.44	3.67	3.61	3.53

7.3 Temperature Effect

Reaction or exposure time of 30 minutes was used for both CO_2 adsorption and methanation that was continued until the CH_4 value decreased below 1000 ppm. Both CO_2 (and consequently CH_4) were slightly reduced as the temperature increased consistent with thermodynamics for exothermic reactions favorable at lower temperature. Results of the temperature effect from the parametric study are shown in Figure 7.3.

No obvious initiation delay of methanation was observed indicating the temperature range was sufficient for the methanation reaction to proceed. Desorption of CO_2 increased with temperature consistent with its endothermic nature. Carbon balances were 80.06%, 95.02%, 98.96%, 97.60 and 108.12% for temperatures increasing from 250 °C to 350 °C.

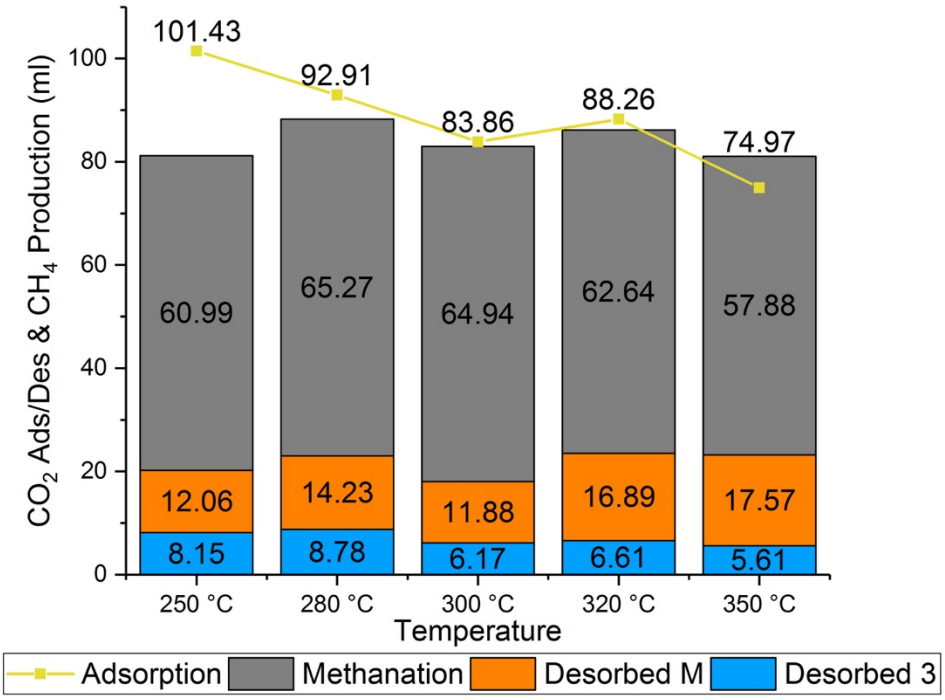

Figure 7.3 Parametric results with simulated flue gas for 10 g of tablet DFM in the fixed bed reactor for various temperatures at 1042 h^{-1}. Nomenclature is same as Figure 7.1.

The amount of CO_2 adsorbed at 250 °C was larger than all other temperatures but the rate of methanation was low. A portion of the adsorbed CO_2 was not methanated and remained on the sample surface in the form of carbonate. This can explain the low carbon balance of 80% at 250 °C while all other carbon balances at higher temperatures were acceptable. Lower methane was generated at 350 °C due to lower CO_2 adsorption consistent with thermodynamics.

7.4 CO_2 Adsorption Duration Effect: Impact of O_2 on Ru

An important conclusion from our published paper [148] was that the O_2-containing CO_2 feed flow rate affects the duration of Ru exposure which effects the extent to which Ru is oxidized. The longer the exposure time the greater extent of Ru oxidation which delays the rate of reduction to metallic Ru once H_2 is added. 5% H_2 was proven (see chapter 5) not sufficient to rapidly reduce the RuO_x and initiate methanation. To insure reduction of the RuO_x, 15% H_2 / N_2 determined to be sufficient to reduce RuO_x to Ru metal, was successfully used for all parametric and aging studies. Figure 7.4 and Figure 7.5 show the results of CO_2 adsorption duration and the CH_4 production vs. time, respectively.

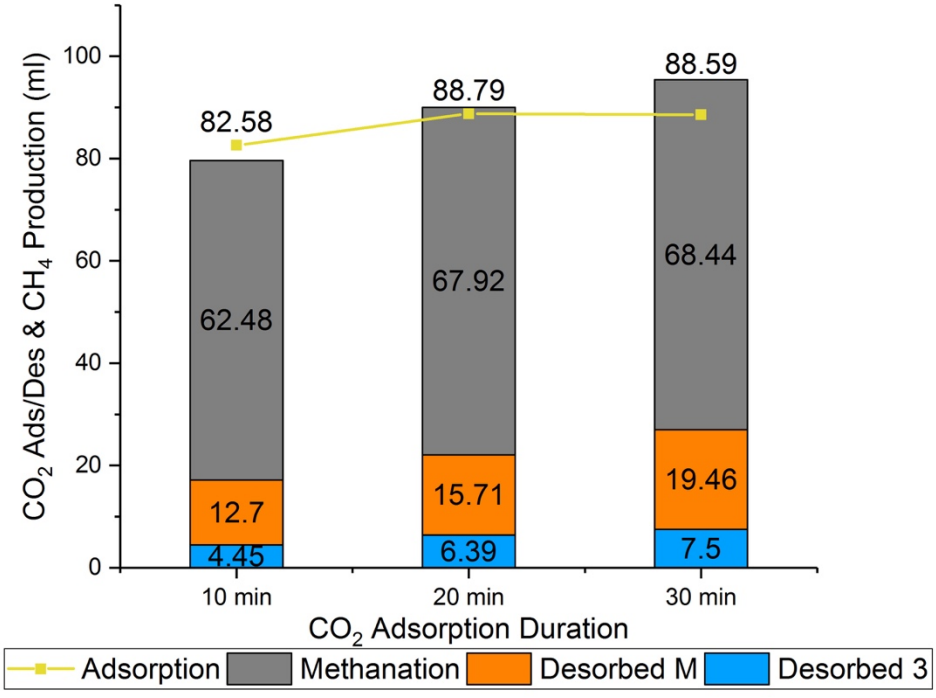

Figure 7.4 Parametric results with simulated flue gas for 10 g of tablet DFM in the fixed bed reactor for varied CO_2 adsorption duration at 320 ℃, 868 h^{-1}. Nomenclature is same as Figure 7.1.

CO_2 adsorption was initially enhanced with increased exposure duration (or reaction time) but reached a plateau after about 20 minutes. Methane production also increased slightly with increased duration exposure as more CO_2 was adsorbed and available for reaction. Desorbed CO_2 also increased which suggests it might be necessary to install a Ru / Al_2O_3 catalyst downstream to complete methanation. Material balances increased with duration time from 96.43% and 101.39% to 107.69% for 10 min, 20 min and 30 min.

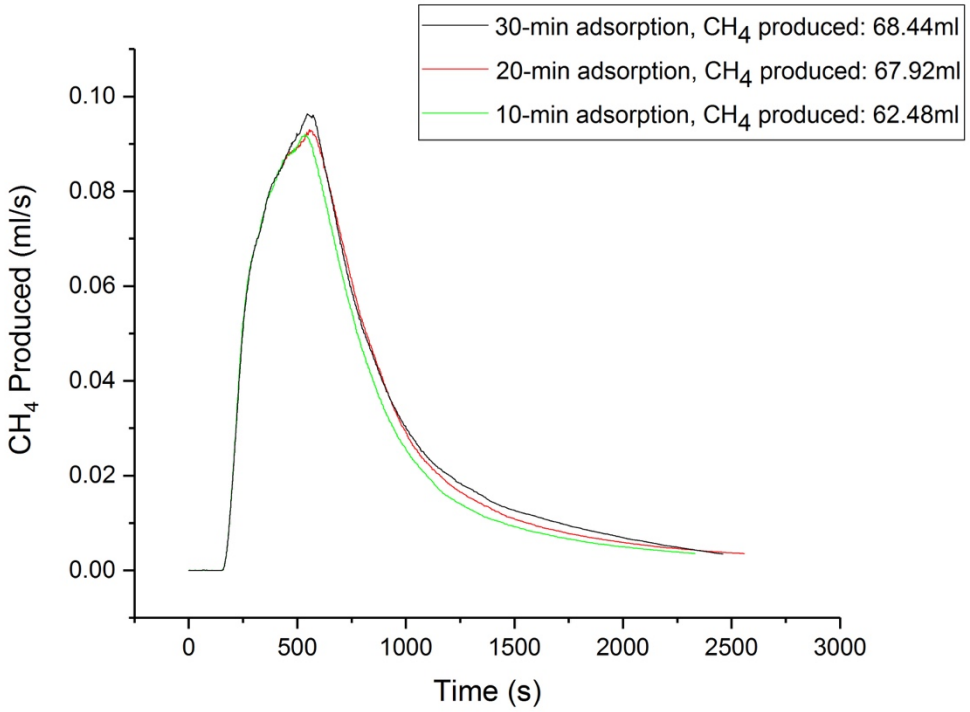

Figure 7.5 CH_4 production vs. time of exposure in simulated flue gas for adsorption for different duration times, 320 ℃, 868 h^{-1}, 1 atm., 15% H_2 / N_2.

O_2 consumptions from 10 to 30 min adsorption are 59.41 ml, 67.86 ml and 66.71 ml, which corresponds to the extent of oxidation of Ru in the DFM. Upon exposure to simulated flue gas, Ru oxidation reached a plateau with no further reaction. However, no delay in the initiation of methanation was observed when adsorption duration was prolonged. This indicates that 15% H_2 / N_2 provides a sufficient reductive environment for the oxidized Ru to be reduced to active metallic Ru.

Chapter 8: Long Term Multi-Cyclic Aging Study of Tablet DFM

Following the parametric study, the same 10-gram sample was subjected to a long term cyclic aging study in the scale-up fixed bed reactor. The aging study was conducted to determine DFM stability, and to explore preliminary operational conditions for a future commercial swing reactor process. Parallel swing reactors switch functions for CO_2 capture and catalytic conversion allowing for continuous operation.

Fifty cycles (cycle = adsorption of CO_2, N_2 purge and methanation) were conducted under conditions derived from the results of the parametric study. The operational conditions were 15 min of CO_2 adsorption, in simulated flue gas at a GHSV of 521 h^{-1}, a 3-min pure N_2 purge followed by 15 minutes of 15% H_2 / N_2 flow for methanation at GHSV of 1389 h^{-1}, 300 °C, 1 atm.

8.1 Stability in the Aging Study

The results of the cyclic aging study are shown in Figure 8.1 in which the performance is averaged from each of 10 cycles. A key result is there is no deactivation observed after 50 cycles. Additionally, since the same 10-gram sample was also used in the prior parametric tests the aging corresponded to about 80 hours of time on stream. Averaged carbon balances for every 10 cycles were 98.37%, 104.97%, 104.13%, 104.52% and 107.85%.

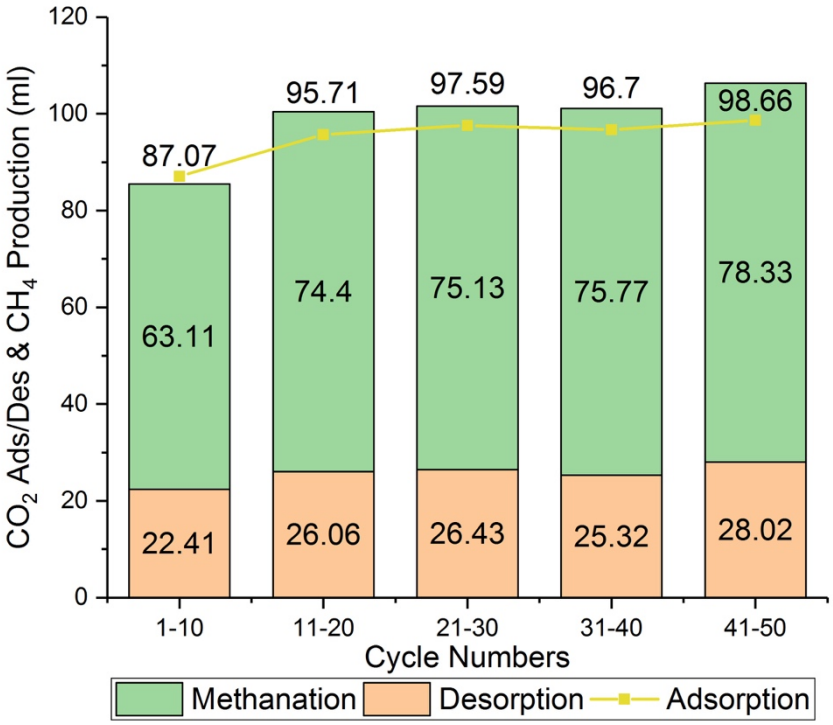

Figure 8.1 Aging study results of averaged CO_2 adsorption, CO_2 desorption and CH_4 production for every 10 cycles. Operational conditions: 15 min for adsorption in simulated flue gas at 521 h^{-1}, 15 min for methanation in 15% H_2 / N_2 at 1389 h^{-1}, with 3 min of pure N_2 purge between each step, 300 ℃, 1 atm.

8.2 BET and H_2 Chemisorption for Fresh and Aged Tablet DFM

BET specific surface area (Table 8.1) showed little or no difference between fresh and aged tablet DFM within experimental error confirming no loss in BET surface area. Samples for H_2 chemisorption were pre-reduced in 10% H_2 / N_2 at 320 °C for 21 hours (fresh, to thoroughly reduce Ru and decompose Na_2CO_3) and 1 hours (aged, to reduce any oxidized Ru and adsorbed CO_2 from cyclic aging tests) prior to chemisorption. Both Ru dispersion and averaged Ru crystallite size were derived from H_2 chemisorption tests.

Table 8.1 BET surface area and Ru dispersion results derived from H_2 chemisorption for both fresh and aged DFM tablets.

Sample	CO_2 uptake / "Na_2O" site (mmol/mmol)	BET Surface Area (m^2/g)	Ru Dispersion (%)	Averaged Ru Crystallite Size (nm)
Fresh	0.36	101.1	3.90	13.9
Aged	0.40	99.23	7.19	6.20

An increase in Ru dispersion from fresh to aged tablet DFM was observed. It is speculated that the aged DFM was further activated during the parametric and aging studies by repeatedly being oxidized and reduced enhancing the apparent metal and adsorbent dispersion of aged verses the fresh sample. It is likely that NaOH is produced from the water in the simulated flue gas that reacts with "Na_2O" in the DFM. Under the operation temperature of the parametric and aging studies (~300 °C) and with the additional heat generated during methanation, the NaOH is likely melted (bulk melting point 318 °C, might be lower when supported) during CO_2 capture which then diffuses on the DFM surface enhancing the adsorbent dispersion. The Ru re-dispersion was verified by TEM measurements (Figure 8.3 and 8.4) studies. The major conclusion is that no decline in performance or characterization data suggests any deactivation of the DFM.

8.3 X-ray Diffraction (XRD) Pattern

X-ray Diffraction patterns were performed with the fresh and aged ground DFM tablets, with comparison of bulk Na_2CO_3 and γ-Al_2O_3 powder, see Figure 8.2. No significant peaks corresponding to bulk Na_2CO_3 are evident indicating the impregnated Na_2CO_3 is essentially

amorphous. The representative peaks (at 2θ of 38°, 46° and 66°) associated with the γ-Al_2O_3 carrier were retained for both the ground DFM tablet patterns.

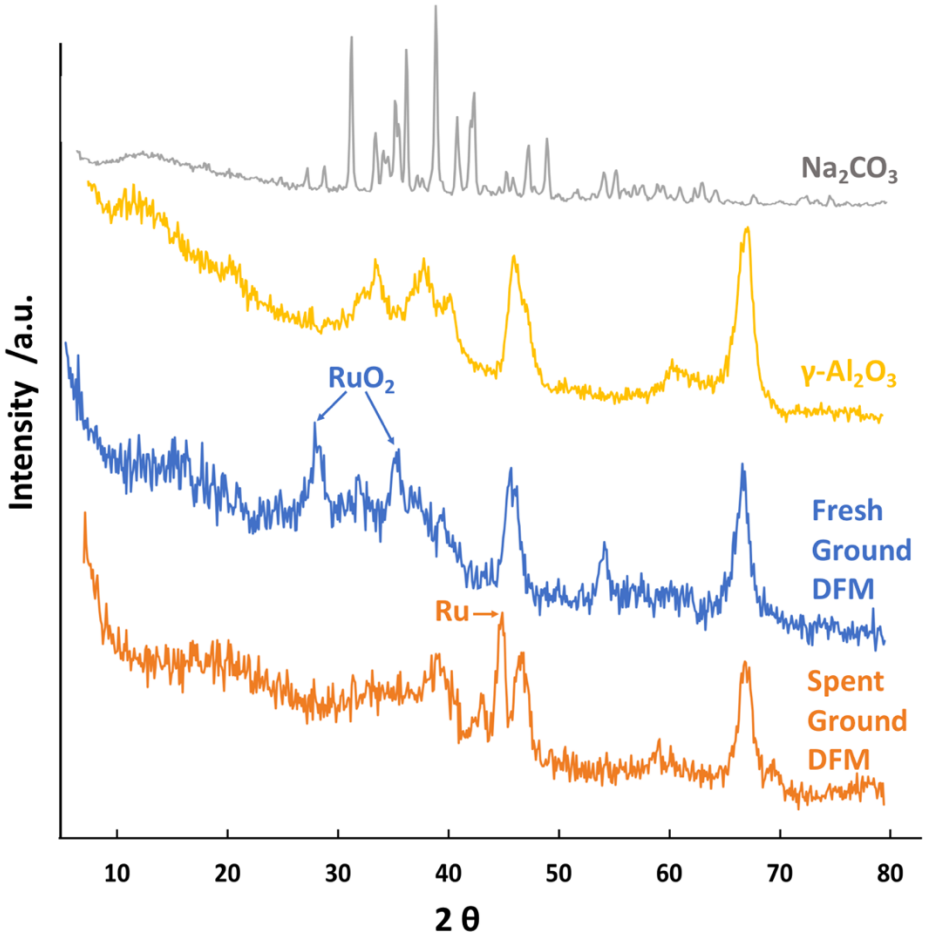

Figure 8.2 X-ray diffraction patterns for the fresh and aged ground DFM tablets, with comparison of bulk Na_2CO_3 and γ-Al_2O_3 powder.

In the ground fresh DFM tablet pattern, peaks located at 2θ of 27° and 35° are associated with RuO_2 (110) and RuO_2 (101), respectively [150]. RuO_2 is formed mainly in the calcination step in air during material preparation. These two peaks vanished in the aged DFM tablet pattern indicates no RuO_2 is visible after exposure to H_2 atmosphere for sufficient time and been

thoroughly reduced to metallic Ru. The peak shown in the aged DFM pattern at 2θ of 43° corresponds to Ru (200) [150] indicating metallic Ru was present.

No peaks responsible for any sodium species were detected in these XRD patterns. This indicates its amorphous nature in the DFM. The hydrogenation of supported Na_2CO_3 to what is speculated to be "Na_2O" was presented earlier (section 4.1) in this thesis. Since the aged DFM was exposed to simulated flue gas containing steam and the methanation reaction itself generates water, the sodium species is probably NaOH. The peak at 2θ of 54° in the fresh DFM pattern is unknown.

8.4 Transmission Electron Microscopy (TEM) Image and Energy-dispersive X-ray Spectroscopy (EDS) Mapping

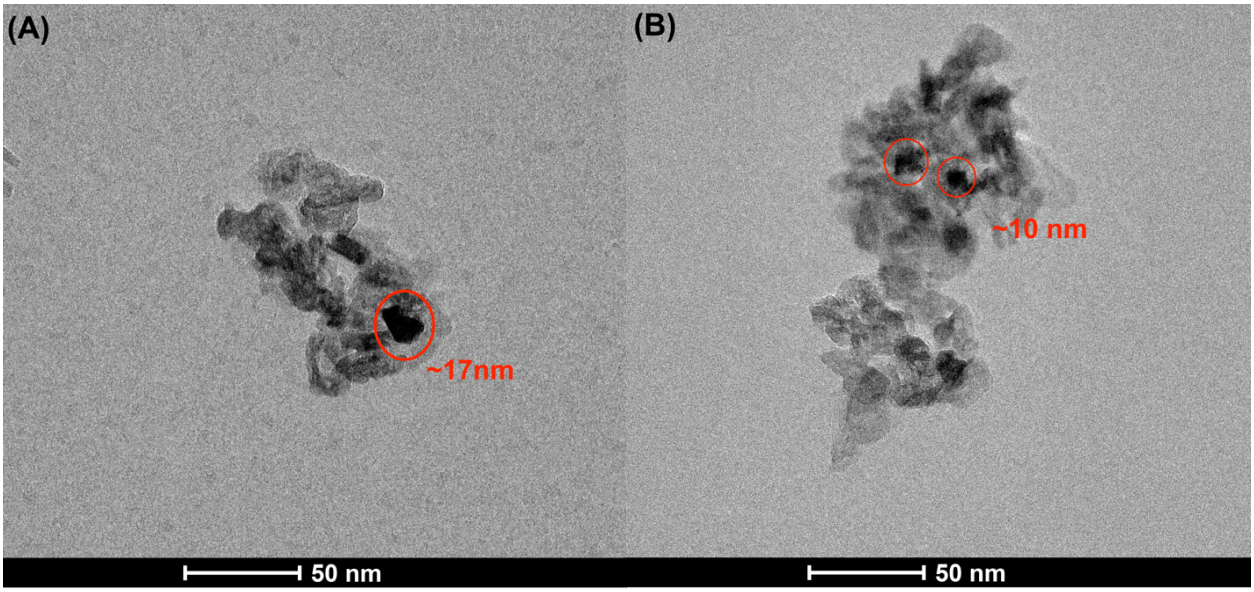

Figure 8.3 TEM images of the fresh (A) and aged (B) ground DFM sample. Area encircled in red is identified as Ru-containing cluster with its estimated size.

Fresh and aged DFM tablets were ground to fine powders to obtain the TEM images, see Figure 8.3. The red circles highlight the Ru cluster in the sample (~ 17 nm in Figure 8.3 A and ~10 nm in Figure 8.3 B).

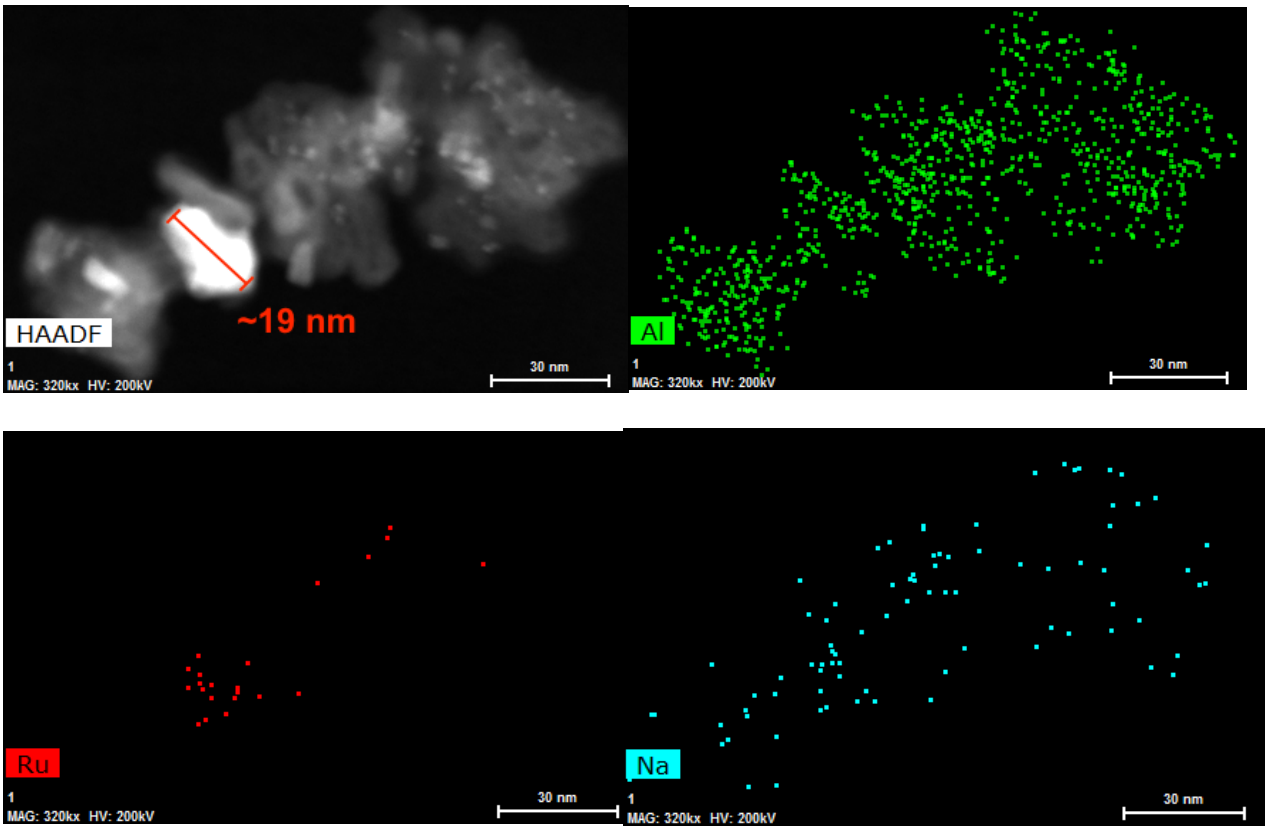

Figure 8.4 STEM-EDS Mapping for the ground fresh DFM tablet sample. Area encircled in red is identified as Ru-containing cluster with its estimated size.

STEM-EDS mapping was sued to recognize Ru-containing particle size of which the results are shown in Figure 8.4 and 8.5 for fresh and aged ground DFM tablets, respectively. The red circles highlight the Ru cluster in the scanned particle. From the H_2 chemisorption results (section 8.2), the averaged Ru crystallite size for fresh and aged samples are calculated to be 13.9 nm and 6.2 nm. Based on the Ru scattering in both Figure 8.4 and 8.5, the highlighted part can be

recognized as the Ru cluster, and their sizes are 19 nm and 10 nm consistent with the decreasing trend in Ru particle size. The repeated oxidation and reduction of the RuO_x/Ru suggests the size decrease appears to be caused by Ru re-dispersion during the 50 cycles.

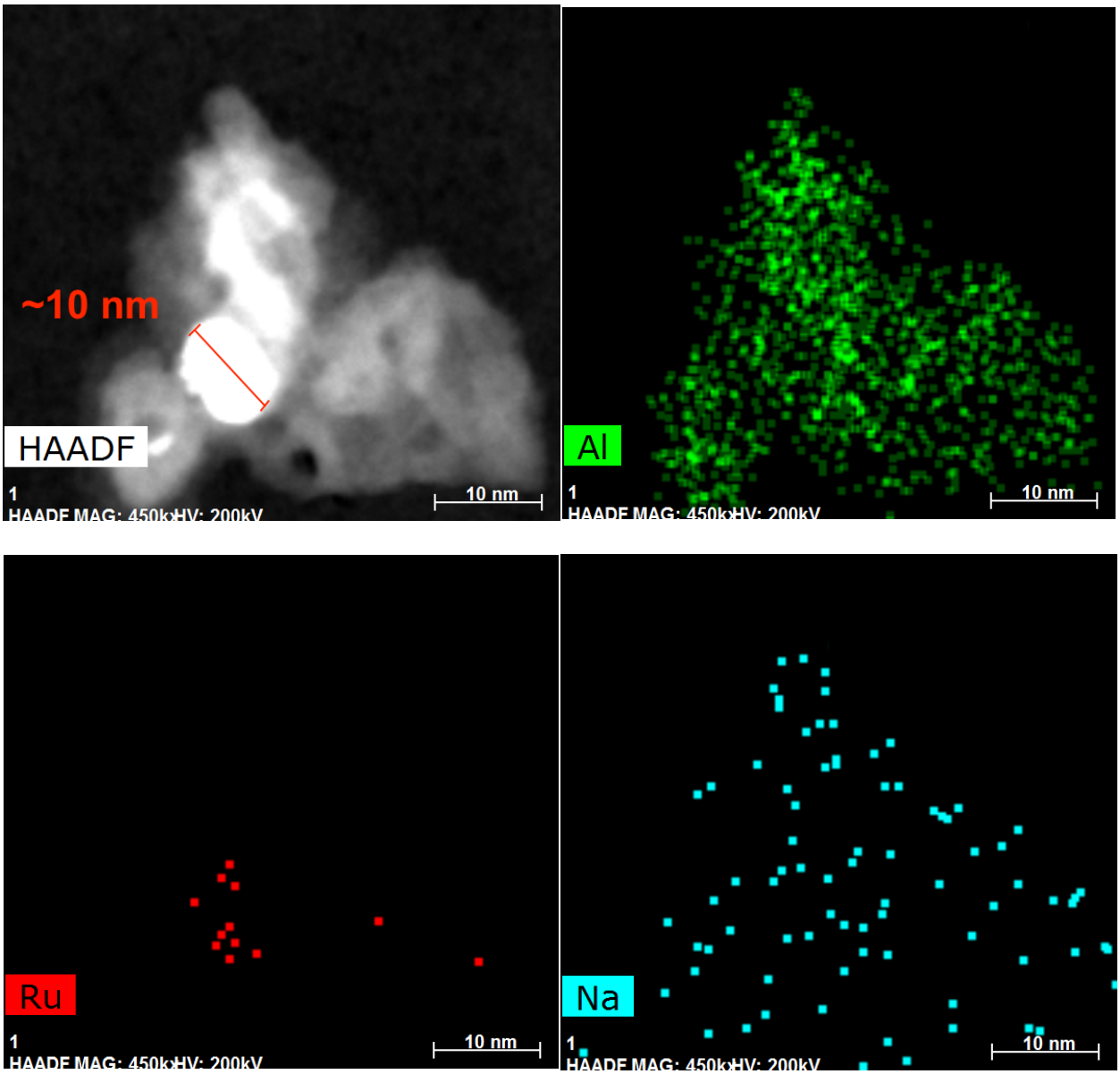

Figure 8.5 STEM-EDS Mapping for the ground aged DFM tablet sample. Area enriched in red is the Ru-containing cluster.

Chapter 9 Thesis Conclusion and Future Work

9.1 Thesis Conclusion

The second generation of dual functional materials (DFM) consisting of solid CO_2 adsorbent ("Na_2O" from hydrogenated Al_2O_3-supported Na_2CO_3) and metallic catalyst (Ru) was developed and demonstrated to capture CO_2 from a simulated natural gas fueled power plant flue gas (O_2- and steam-containing) and catalytically converted to synthetic natural gas (CH_4). The new DFM was demonstrated to have excellent adsorption and catalytic activity and stability, as demonstrated in the 50 aging cycles and 80 hours of operation. The Ru underwent continuous oxidation and reduction during the aging test and maintained stable high activity and a slight increase in dispersion. Stable performance was further confirmed by stable surface area (BET), chemisorption measurements and TEM images.

Studies initially conducted with DFM powders were scaled up to 5 mm × 5 mm tablets to a structure suitable for future commercial use and fixed bed aging. One can envision a commercial process operating in a swing bed mode where each bed alternates between adsorption and methanation for continuous CO_2 capture and methane production.

The synthetic natural gas product can be either recycled to the inlet of the power plant for re-combustion or integrated into the existed natural gas infrastructures (pipeline) to achieve a closed carbon cycle. This study offers a unique solution for the current environment-energy crises by providing a combined approach for CO_2 emission control with a sustainable fuel supply. By capturing and converting CO_2 in situ, the conventional CO_2 liquid amine sorbent technology and its energy intensive regeneration step are eliminated, together with the avoidance of operation- and infrastructure-related problems such as toxicity and corrosion. Also, CO_2 storage and

transportation issues are eliminated because the converted CO_2 can be consumed as CH_4 at the emission location.

H_2 exposure intensity plays an important role in the new DFM hydrogenation of the reformed carbonate (captured CO_2) and stability controlled by longer exposure time or H_2 increased partial pressure. It also maintains Ru in its active metallic state after oxidation during the CO_2 adsorption step. Parametric studies identified an optimized operational condition where H_2 partial pressure ensures continuous and stable performance.

A fundamental operational mechanism of DFM was identified by kinetic studies allowing an empirical rate law (Equation 6.3) to be established. H_2 partial pressure possesses a higher reaction order (~1) indicating its dominant impact on the rate of the methanation step rate, while CO_2 coverage on the DFM surface showed essentially zero reaction order indicative of no impact on the overall rate of the methanation step. The lower activation energy calculated is attributed to the co-effect of kinetics and diffusion for controlling the rate of the methanation process. Some internal pore diffusion of desorbed CO_2 from the "Na_2O" sites diffusing to the Ru sites for methanation is speculated to give an activation energy about ½ that of Ru / Al_2O_3 alone.

A parametric study was conducted with 10 grams of 5 mm × 5 mm DFM tablets to establish optimum conditions for aging tests and to provide guidance for future commercial use. Both CO_2 adsorption capacity and CH_4 produced were positively impacted by changing the flow rates. Most importantly the duration of the adsorption step impacts the exposure of Ru to O_2 in the feed gas, influencing the extent to which Ru is oxidized. Its reduction is and thus the 15% H_2 partial pressure is critical to maintain Ru in its metallic and active state during methanation. The impact of operational temperature for adsorption is consistent with thermodynamic; lower temperatures

improve CO_2 capture capacity but does not kinetically favored methanation. Higher temperature facilitates methanation kinetics but also enhances the endothermic desorption of adsorbed CO_2.

Overall this thesis identified a key second generation DFM material and the key kinetic parameters necessary for demonstrating stable performance in a 50-cycle aging study composed of adsorption of CO_2, from a simulated O_2-containing flue gas, followed by methanation. Stable cyclic performance was consistent with BET, H_2 chemisorption and TEM results.

9.2 Future Work

A developed technology was shown feasible for CO_2 capture and in situ catalytic conversion to methane using a newly discovered second generation dual functional material (DFM). The capacity of CO_2 capture and CH_4 production requires the use of renewable H_2 for possible future application in O_2- and steam-containing power plant flue gas. To further improve this technology the following suggestions for future work are indicated below.

9.2.1 Further DFM Optimization by New Components

Although the second generation of DFM for both the CO_2 adsorption capacity and CH_4 production have been significantly improved, the technology can be further developed with continuous exploration of new and effective CO_2 adsorbents and carrier materials. In particular, alternatives to Al_2O_3 as the DFM carrier and high surface area alkaline zeolites should be investigated for new CO_2 adsorption material.

This thesis has shown that Ru has outstanding performance in activity, selectivity and stability for the CO_2 adsorption and methanation functions, and its chemical redox property for O_2-containing flue gas applications. Some optimization from the current 5% loading will improve

its cost effectiveness (Ru is a precious metal at ~ $1.50 / gram) while controlling the rate of methanation reaction and the heat liberated necessary to control the bed temperature. Some base metal additions may permit an optimized loading of Ru will be explored.

9.2.2 Further Scale Up and a Swing Reactor System

10 grams of tablet DFM has been successfully tested and optimal operational conditions determined that provides suggestion for larger scale applications and for a more continuous swing reactor design. A mini pilot plant with much larger capacity needs to be constructed for further scale up of the technology. A swing reactor system that allows continuous operation of both CO_2 capture and methanation is a necessary step for this technology to be further advanced.

9.2.3 Actual Flue Gas Situation and Poisoning

In this thesis, the CO_2 feed gas is either diluted CO_2 / N_2 or simulated flue gas that contains a purified composition of typical natural gas fueled power plant flue gas. In actual industrial applications, poisoning components, such as SO_x and NO_x, even in trace amounts, can have a poisoning effect on the catalytic materials and the adsorbents. Power plants are equipped with pollution abatement such as Flue-Gas Desulfurization (FGD) for SO_x and Selective Catalytic Reduction (SCR) for NO_x reduction, upstream but the DFM is likely to be exposed to traces of these constituents and thus their impact on performance must be determined. If required regeneration methods must be developed and/or guard beds identified to protect the DFM. A real flue gas from a natural gas powered appliance will be used in the laboratory to bring us closer to a power plant effluent.

9.2.4 Verification of the Na_2O existence

A better understanding of the Al_2O_3-supported Na_2CO_3 decomposition, at intermediate temperature (> 135 °C) has been reported [144]. In this thesis we have studied its hydrogenation in the presence of a metallic Ru catalyst. However, more solid proof for the existence of the "Na_2O" in the current work, would be fundamentally useful.

X-ray diffraction (XRD) test showed no peak corresponding to Na_2O, NaOH nor Na_2CO_3 suggesting these are likely dispersed amorphously and cannot be detected by the XRD. More advanced characterization methods, such as in situ FTIR, could be more effective for studying this.

9.2.5 Industrial Partner

We would like to have an industrial partner with whom we can work to further advance the testing, economics and a real process for DFM. This will be an important future challenge as we further establish laboratory feasibility.

References

1. IPCC Second Assessment Climate Change 1995: A Report Of The Intergovernmental Panel On Climate Chance. Available at: https://www.ipcc.ch/pdf/climate-changes-1995/ipcc-2nd-assessment/2nd-assessment-en.pdf

2. Fujimura, S., Shi, P., Iwama, K., Zhang, X., Gopal, J., & Jitsuyama, Y. (2012). Effects of CO_2 Increase on Wheat Growth and Yield under Different Atmospheric Pressures and Their Interaction with Temperature. *Plant Production Science*, 15(2), 118–124.

3. Pereira, K. C., Costa, P. M., Costa, M. H., Luque, Á., DelValls, T. A., & López, I. R. (2016). Effects of the increase of temperature and CO_2 concentration on polychaetae Nereis diversicolor: simulating extreme scenarios of climate change in marine sediments. *Hydrobiologia*, 772(1), 161–174.

4. Hammar, H., & Sjöström, M. (2011). Accounting for behavioral effects of increases in the carbon dioxide (CO_2) tax in revenue estimation in Sweden. *Energy Policy*, 39(10), 6672–6676.

5. The twenty-first session of the Conference of the Parties (COP) and the eleventh session of the Conference of the Parties serving as the meeting of the Parties to the Kyoto Protocol (CMP) took place from 30 November to 11 December 2015, in Paris, France.

6. Boden, T.A., G. Marland, and R.J. Andres. 2010. Global, Regional, and National Fossil-Fuel CO_2 Emissions. Carbon Dioxide Information Analysis Center, Oak Ridge National Laboratory, U.S. Department of Energy, Oak Ridge, Tenn., U.S.A.

7. United Nations Framework Convention on Climate Change (UNFCC). Report of the Conference of the Parties on its Fifteenth Session, held in Copenhagen from 7 to 19 December 2009. Part Two: Action taken by the Conference of the Parties at its Fifteenth Session. United Nations Climate Change Conf. Report 43. (UNFCC, 2009)
Available at: http:// unfccc.int/resource/docs/2009/cop15/eng/11a01.pdf

8. McGlade, C., & Ekins, P. (2015). The geographical distribution of fossil fuels unused when limiting global warming to 2 °C. *Nature*, 517, 187.

9. Pacala, S., & Socolow, R. (2004). Stabilization Wedges: Solving the Climate Problem for the Next 50 Years with Current Technologies. *Science*, 305(5686), 968-972.

10. Saidi, M., Heidarinejad, S., Rahimpour, H.R., Talaghat, M.R., Rahimpour, M.R., 2014. Mathematical modeling of carbon dioxide removal using amine-promoted hot potassium carbonate in a hollow fiber membrane contactor. *J. Nat. Gas Sci. Eng*. 18, 274-285.

11. Ahmadpour, E., Shamsabadi, A.A., Behbahani, R.M., Aghajani, M., Kargari, A., 2014. Study of CO_2 separation with PVC/Pebax composite membrane. *J. Nat. Gas Sci. Eng*. 21, 518-523.

12. Miguel, C.V., Soria, M.A., Mendes, A., Madeira, L.M., 2015. Direct CO_2 hydrogenation to methane or methanol from post-combustion exhaust streams - a thermody- namic study. *J. Nat. Gas Sci. Eng*. 22, 1-8.

13. Sheng, J. J. (2015). Enhanced oil recovery in shale reservoirs by gas injection. *Journal of Natural Gas Science and Engineering*, 22, 252–259.

14. Rochelle, G.T., Amine Scrubbing for CO_2 Capture. *Science*, 2009. 325: p. 1652-1654.

15. Leung, D.Y.C., G. Caramanna, and M.M. Maroto-Valer, An overview of current status of carbon dioxide capture and storage technologies. *Renewable and Sustainable Energy Reviews*, 2014. 39: p. 426-443.

16. M. Rukhylyarova, T. Lunkenbein, K. Kahler, R. Schlogl; *Catalyst Letters* (2017) 147; 416-427.

17. Duyar, M. S., Treviño, M. A. A., & Farrauto, R. J. (2015). Dual function materials for CO_2 capture and conversion using renewable H_2. *Applied Catalysis B: Environmental*, 168, 370–376.

18. Duyar, M. S., Wang, S., Arellano-Trevino, M. A., & Farrauto, R. J. (2016). CO_2 utilization with a novel dual function material (DFM) for capture and catalytic conversion to synthetic natural gas: An update. *Journal of CO_2 Utilization*, 15, 65–71.

19. GISS Surface Temperature Analysis (GISTEMP), National Aeronautics and Sapce Administration, Goddard Institute for Sapce Studies.
Available at: http://data.giss.nasa.gov/gistemp/

20. Levitus, S., J. I. Antonov, T. P. Boyer, R. A. Locarnini, H. E. Garcia, and A. V. Mishonov (2009), Global ocean heat content 1955–2008 in light of recently revealed instrumentation problems, *Geophys. Res. Lett.*, 36, L07608.

21. World Glacier Monitoring Service, under the auspices of: ICSU (WDS), IUGG (IACS), UNESCO, WMO. Available at: http://wgms.ch

22. L. Polyak, et.al., "History of Sea Ice in the Arctic," in Past Climate Variability and Change in the Arctic and at High Latitudes, U.S. Geological Survey, Climate Change Science Program Synthesis and Assessment Product 1.2, January 2009, chapter 7

23. Church, J. A. and N.J. White (2006), A 20th century acceleration in global sea level rise, *Geophysical Research Letters*, 33, L01602.

24. Daniel P Aldrich. The Right Way to Build Resilience to Climate Change. *Current History (2018)*. 16-21.

25. Kirppu, H., Lahdelma, R., & Salminen, P. (2018). Multicriteria evaluation of carbon-neutral heat-only production technologies for district heating. *Applied Thermal Engineering*, 130, 466–476.

26. Tattini, J., Gargiulo, M., & Karlsson, K. (2018). Reaching carbon neutral transport sector in Denmark - Evidence from the incorporation of modal shift into the TIMES energy system modeling framework. *Energy Policy*, 113, 571–583.

27. Pierucci, A., Cannavale, A., Martellotta, F., & Fiorito, F. (2018). Smart windows for carbon neutral buildings: A life cycle approach. *Energy and Buildings*, 165, 160–171.

28. Gutiérrez, A. S., Eras, J. J. C., Huisingh, D., Vandecasteele, C., & Hens, L. (2018). The current potential of low-carbon economy and biomass-based electricity in Cuba. The case of sugarcane, energy cane and marabu (Dichrostachys cinerea) as biomass sources. *Journal of Cleaner Production*, 172, 2108–2122.

29. Mondal M. K., Balsora H. K., Varshney P. Progress and trends in CO_2 capture/separation technologies: a review. *Energy 2012*;46:431–41.

30. Guan, G. (2017). Clean coal technologies in Japan: A review. *Chinese Journal of Chemical Engineering*, 25(6), 689–697.

31. Merkel, T. C., Lin, H., Wei, X., & Baker, R. (2010). Power plant post-combustion carbon dioxide capture: An opportunity for membranes. *Journal of Membrane Science*, 359(1), 126–139.

32. Samanta, A., Zhao, A., Shimizu, G. K. H., Sarkar, P., & Gupta, R. (2012). Post-Combustion CO_2 Capture Using Solid Sorbents : A Review. *Industrial & Engineering Chemistry Research*, 51, 1438–1463.

33. Do, D. D.; Wang, K. A new model for the description of adsorption kinetics in heterogeneous activated carbon. *Carbon 1998*, 36, 1539–1554.

34. Mugge J.; Bosch, H.; Reith, T. Gas Adsorption kinetics in activated carbon. In Adsorption Science and Technology: Proceedings of the Second Pacific Basin on Adsorption Science and Technology, 2nd, Brisbane, Australia, May 14 18, 2000; pp 451-455.

35. Radosz, M.; Hu, X.; Krutkrarnelis, K.; Shen, Y. Flue-gas carbon capture on carbonaceous sorbents: toward a low-cost multifunctional carbon filter for “green” energy producers. *Ind. Eng. Chem. Res.* 2008, 47, 3783–3794.

36. Furukawa,H.; Ko,N.; Go,Y.B.; Aratani,N.; Choi,S.B.; Choi, E.; Yazaydin, A. O.; Snurr, R. Q.; O'Keeffe, M.; Kim, J.; Yaghi, O. M. Ultrahigh porosity in metal-organic frameworks. *Science* 2010, 329, 424–428.

37. Hoffman, J. S.; Pennline, H. W. Study of regenerable sorbents for CO_2 capture. In Proceedings of First National Conference on Carbon Sequestration, Washington, DC, May 2001.

38. Hayashi, H.; Taniuchi, J.; Furuyashiki, N.; Sugiyama, S.; Hirano, S.; Shigemoto, N.; Nonaka, T. Efficient recovery of carbon dioxide from flue gases of coal-fired power plants by cyclic fixed-bed operations over K_2CO_3-on-carbon. *Ind. Eng. Chem. Res*. 1998, 37, 185–191.

39. Seo, Y.; Jo, S. H.; Ryu, C. K.; Yi, C. K. Effects of water vapor pretreatment time and reaction temperature on CO_2 capture characteristics of a sodium-based solid sorbent in a bubbling fluidized-bed reactor. *Chemosphere* 2007, 69, 712–718.

40. Lee, J. B.; Ryu, C. K.; Baek, J. I.; Lee, J. H.; Eom, T. H.; Kim, S. H. Sodium-based dry regenerable sorbent for carbon dioxide capture from power plant flue gas. *Ind. Eng. Chem. Res*. 2008, 47, 4465–4472.

41. Lee, S. C.; Choi, B. Y.; Lee, T. J.; Ryu, C. K.; Ahn, Y. S.; Kim, J. C. CO_2 absorption and regeneration of alkali metal-based solid sorbents. *Catal. Today* 2006, 111, 385–390.

42. Lee, S. C.; Kim, J. C. Dry potassium-based sorbents for CO_2 capture. *Catal. Surv. Asia* 2007, 11, 171–185.

43. Lee, S. C.; Chae, H. J.; Lee, S. J.; Parka, Y. H.; Ryu, C. K.; Yi, C. K.; Kim, J. C. Novel regenerable potassium-based dry sorbents for CO_2 capture at low temperatures. *J. Mol. Catal. B* 2009, 56, 179–184.

44. Lee, S. C.; Choi, B. Y.; Ryu, C. K.; Ahn, Y. S.; Lee, T. J.; Kim, J. C. The effect of water on the activation and the CO_2 capture capacities of alkali metal-based sorbents. *Korean J. Chem. Eng*. 2006, 23, 374–379.

45. Lee, S. C.; Kwon, Y. M.; Ryu, C. Y.; Chae, H. J.; Ragupathy, D.; Jung, S. Y.; Lee, J. B.; Ryu, C. K.; Kim, J. C. Development of new alumina-modified sorbents for CO_2 sorption and regeneration at temperatures below 200 °C. *Fuel* 2011, 60, 1465–1470.

46. Zhao, C.; Chen, X.; Zhao, C. CO_2 absorption using dry potassium-based sorbents with different supports. *Energy Fuels* 2009, 23, 4683–4687.

47. Green, D. A.; Nelson, T. O.; Turk, B. S.; Box, P. D.; Gupta, R. P. Carbon dioxide capture from flue gas using dry regenerable sorbents. DOE Cooperative Agreement No. DE-FC26-00NT40923, 2006.

48. Nelson, T. O.; Green, D. A.; Box, P. D.; Weber, A.; Gupta, R. P. Production of concentrated CO_2 from flue gas using dry regenerable carbonate sorbents in a thermal-swing process. Presented at the Fifth Annual Conference on Carbon Capture and Sequestration, Alexandria, VA, USA, May 8 11, 2006.
Available at: http://www.netl.doe.gov/publications/proceedings/06/carbon-seq/Tech%20Session%20009.pdf

49. Nelson, T. O. The Dry Carbonate Process: Carbon Dioxide Recovery from Power Plant Flue Gas. Annual NETL Capture Technol- ogy for Existing Power Plant R&D Meeting, Pittsburgh, PA, March 24 26, 2009.
Available at: http://www.netl.doe.gov/ publications/proceedings/09/CO2/pdfs/43089%20RTI%20sorbent%20(Nelson)%20mar09.pdf.

50. Yi,C.K.; Jo,S.H.; Seo,Y.; Lee,J.B.; Ryu,C.K. Continuous operation of the potassium-based dry sorbent CO2 capture process with two fluidized-bed reactors. *Int. J. Greenhouse Gas Control* 2007, 1, 31–36.

51. Yi,C.K. Development of CO_2 capture technology using solid sorbents. Presented at APP (Asia Pacific Partnership), Power Generation and Transmission Task Force Meeting, July 7, 2009, Seoul, Korea.

52. Park,Y.C.; Jo,S.H.; Ryu,C.K.; Yi,C.K. Long-termoperation of carbon dioxide capture system from a real coal-fired flue gas using dry regenerable potassium-based sorbents. *Energy Procedia* 2009, 1, 1235–1239.

53. Przepiorski, J.; Skrodzewicz, M.; Morawski, A. W. High temperature ammonia treatment of activated carbon for enhancement of CO_2 adsorption. *Appl. Surf. Sci*. 2004, 225, 235–242.

54. Jadhav, P. D.; Chatti, R. V.; Biniwale, R. B.; Labhsetwar, N. K.; Devotta, S.; Rayalu, S. S. Monoethanol amine modified zeolite 13X for CO_2 adsorption at different temperatures. *Energy Fuels* 2007, 21, 3555–3559.

55. Su, F.; Lu, C.; Kuo, S. C.; Zeng, W. Adsorption of CO2 on amine-functionalized Y-type zeolites. *Energy Fuels* 2010, 24, 1441–1448.

56. Porcheron, F.; Ferre, D.; Favre, E.; Nguyen, P. T.; Lorain, O.; Mercier, R.; Rougeau, L. Hollow Fiber Membrane Contactors for CO_2 Capture: From Lab-Scale Screening to Pilot-Plant Module Con- ception. *Energy Procedia* 2011, 4, 763−770.

57. Ibrahim, M. H., El-Naas, M. H., Zhang, Z., & der Bruggen, B. (2018). CO_2 Capture Using Hollow Fiber Membranes: A Review of Membrane Wetting. *Energy & Fuels*, 32(2), 963–978.

58. Li S, Zhou J, Pyrzynski A, Makkuni A, Meyer H, Ding Y, et al. Hybrid membrane/ absorption process for post-combustion CO_2 capture [Final Technical Report]. 2014.

59. Freeman B, Hao P, Baker R, Kniep J, Chen E, Ding J, et al. Hybrid membrane- absorption CO_2 capture process. *Energy Procedia* 2014;63:605–13.

60. National Energy Technology Laboratory. Carbon dioxide capture from existing coal-fired power plants [Final Report] 2007. (DOE/NETL-401/110907).

61. Van Selow ER, Cobden PD, Wright A, Van den Brink RW, Jansen D. Improved sorbent for the sorption-enhanced water-gas shift process. *Energy Procedia* 2011; 4:1090–5.

62. Ochoafernández E, Haugen G, Zhao T, Rønning M, Aartun I, Børresen B, et al. Process design simulation of H_2 production by sorption enhanced steam methane reforming: evaluation of potential CO_2 acceptors. *Green Chem* 2007;9:654–62.

63. Soria MA, Tosti S, Mendes A, Madeira LM. Enhancing the low temperature water-gas shift reaction through a hybrid sorption-enhanced membrane reactor for high-purity hydrogen production. *Fuel* 2015;159:854–63.

64. Fong JCLY, Anderson CJ, Xiao G, Webley PA, Hoadley AFA. Multi-objective optimisation of a hybrid vacuum swing adsorption and low-temperature post-combustion CO_2 capture. *J Clean Prod* 2016;111:193–203.

65. Shao P, Dal-Cin M, Kumar A, Li H, Singh DP. Design and economics of a hybrid membrane–temperature swing adsorption process for upgrading biogas. *J Membr Sci* 2012;413–414:17–28.

66. Anantharaman R, Berstad D, Roussanaly S. Techno-economic performance of a hybrid membrane –liquefaction process for post-combustion CO_2 capture. *Energy Procedia* 2014;61:1244–7.

67. Belaissaoui B, Moullec YL, Willson D, Favre E. Hybrid membrane cryogenic process for post-combustion CO_2 capture. *J Membr Sci* 2012;415–416:424–34.

68. Kundu PK, Chakma A, Feng X. Effectiveness of membranes and hybrid membrane processes in comparison with absorption using amines for post-combustion CO_2 capture. *Int J Greenh Gas Control* 2014;28:248–56.

69. Surovtseva D, Amin R, Barifcani A. Design and operation of pilot plant for CO_2 capture from IGCC flue gases by combined cryogenic and hydrate method. *Chem Eng Res Des* 2011;89:1752–7.

70. Hasse D, Kulkarni S, Sanders E, Corson E, Tranier J. CO_2 capture by sub-ambient membrane operation. *Energy Procedia* 2013;37:993–1003.

71. Kulkarni SS. CO_2 capture by sub-ambient membrane operation. In: 2012 NETL CO_2 capture technology meeting; July 9 – 12, 2012. NETL Award # DE-FE0004278.

72. Strube R, Manfrida G. CO_2 capture in coal-fired power plants - impact on plant performance. *Int J Greenh Gas Control* 2011;5(4):710–26.

73. Song, C., Liu, Q., Ji, N., Deng, S., Zhao, J., Li, Y., … Li, H. (2018). Alternative pathways for efficient CO2 capture by hybrid processes-A review. *Renewable and Sustainable Energy Reviews*, 82, 215–231.

74. C. G. Visconti, M. Martinelli, L. Falbo, A. Infantes-Molina, L. Lietti, P. Forzatti, G. Iaquaniello, E. Palo, B. Picutti and F. Brignoli, CO_2 hydrogenation to lower olefins on a high surface area K-promoted bulk Fe-catalyst. *Appl. Catal., B*, 2017, 200, 530–542.

75. P. Gao, S. Li, X. Bu, S. Dang, Z. Liu, H. Wang, L. Zhong, M. Qiu, C. Yang, J. Cai, W. Wei and Y. Sun, Direct conversion of CO_2 into liquid fuels with high selectivity over a bifunctional catalyst. *Nat. Chem*., 2017, 9, 1019–1024.

76. H. Song, N. Zhang, C. Zhong, Z. Liu, M. Xiao and H. Gai, Hydrogenation of CO_2 into formic acid using a palladium catalyst on chitin. *New J. Chem*., 2017, 41, 9170–9177.

77. K. Larmier, W.-C. Liao, S. Tada, E. Lam, R. Verel, A. Bansode, A. Urakawa, A. Comas-Vives, C. Copéret, CO_2 - to - Methanol Hydrogenation on Zirconia - Supported Copper Nanoparticles: Reaction Intermediates and the Role of the Metal–Support Interface. *Angew. Chem. Int. Ed*. 2017, 56, 2318.

78. X. Jiang, N. Koizumi, X. Guo and C. Song, Bimetallic Pd-Cu catalysts for selective CO_2 hydrogenation to methanol. *Appl. Catal., B*, 2015, 170–171, 173–185.

79. Kar, S., Sen, R., Goeppert, A., & Prakash, G. K. S. (2018). Integrative CO_2 Capture and Hydrogenation to Methanol with Reusable Catalyst and Amine: Toward a Carbon Neutral Methanol Economy. *Journal of the American Chemical Society*, 140(5), 1580–1583.

80. S. Bai, Q. Shao, P. Wang, Q. Dai, X. Wang and X. Huang, Highly Active and Selective Hydrogenation of CO_2 to Ethanol by Ordered Pd-Cu Nanoparticles. *J. Am. Chem. Soc.*, 2017, 139, 6827–6830.

81. Ma, J., Sun, N., Zhang, X., Zhao, N., Xiao, F., Wei, W., & Sun, Y. (2009). A short review of catalysis for CO2 conversion. *Catalysis Today*, 148(3), 221–231.

82. Jhong, H.-R. "Molly," Ma, S., & Kenis, P. J. A. (2013). Electrochemical conversion of CO_2 to useful chemicals: current status, remaining challenges, and future opportunities. *Current Opinion in Chemical Engineering*, 2(2), 191–199.

83. Hori Y, Wakebe H, Tsukamoto T, Koga O: Electrocatalytic process of CO selectivity in electrochemical reduction of CO_2 at metal–electrodes in aqueous-media. *Electrochim Acta* 1994, 39:1833-1839.

84. Hori Y: CO_2-reduction, catalyzed by metal electrodes. *Handbook of Fuel Cells*. John Wiley & Sons, Ltd.; 2010.

85. Chen Y, Li CW, Kanan MW: Aqueous CO_2 reduction at very low overpotential on oxide-derived Au nanoparticles. *J. Am. Chem. Soc.* 2012, 134:19969-19972.

86. Li CW, Kanan MW: CO_2 reduction at low overpotential on Cu electrodes resulting from the reduction of thick Cu_2O films. *J. Am. Chem. Soc.* 2012, 134:7231-7234.

87. Chen YH, Kanan MW: Tin oxide dependence of the CO_2 reduction efficiency on tin electrodes and enhanced activity for tin/tin oxide thin-film catalysts. *J. Am. Chem. Soc.* 2012, 134:1986-1989.

88. Hinogami R, Yotsuhashi S, Deguchi M, Zenitani Y, Hashiba H, Yamada Y: Electrochemical reduction of carbon dioxide using a copper rubeanate metal organic framework. *ECS Electrochem Lett*. 2012, 1:H17-H19.

89. Tornow CE, Thorson MR, Ma S, Gewirth AA, Kenis PJA: Nitrogen-based catalysts for the electrochemical reduction of CO_2 to CO. *J. Am. Chem. Soc.* 2012, 134:19520-19523.

90. Jhong, H.-R. "Molly," Brushett, F. R., & Kenis, P. J. A. (2013). The Effects of Catalyst Layer Deposition Methodology on Electrode Performance. *Advanced Energy Materials*, 3(5), 589–599.

91. Chang, X., Wang, T., & Gong, J. (2016). CO_2 photo-reduction: insights into CO_2 activation and reaction on surfaces of photocatalysts. *Energy Environ. Sci.*, 9(7), 2177–2196.

92. S. Xie, Q. Zhang, G. Liu and Y. Wang, Photocatalytic and photoelectron catalytic reduction of CO_2 using heterogeneous catalysts with controlled nanostructures. *Chem. Commun.,* 2016, 52, 35–59.

93. W. Tu, Y. Zhou and Z. Zou, Photocatalytic Conversion of CO_2 into Renewable Hydrocarbon Fuels: State-of-the-Art Accomplishment, Challenges, and Prospects. *Adv. Mater.,* 2014, 26, 4607–4626.

94. L. Li, J. Yan, T. Wang, Z. J. Zhao, J. Zhang, J. Gong and N. Guan, Sub-10 nm rutile titanium dioxide nanoparticles for efficient visible-light-driven photocatalytic hydrogen production. *Nat. Commun.*, 2015, 6, 5881.

95. J. C. Wang, L. Zhang, W. X. Fang, J. Ren, Y. Y. Li, H. C. Yao, J. S. Wang and Z. J. Li, Enhanced Photoreduction CO_2 Activity over Direct Z-Scheme α-Fe_2O_3/Cu_2O Heterostructures under Visible Light Irradiation. *ACS Appl. Mater. Interfaces*, 2015, 7, 8631–8639.

96. A. Kudo and Y. Miseki, Heterogeneous photocatalyst materials for water splitting. *Chem. Soc. Rev*., 2009, 38, 253–278.

97. T. Hisatomi, J. Kubota and K. Domen, Recent advances in semiconductors for photocatalytic and photoelectrochemical water splitting. *Chem. Soc. Rev.,* 2014, 43, 7520–7535.

98. Y. Ma, X. Wang, Y. Jia, X. Chen, H. Han and C. Li, Titanium Dioxide-Based Nanomaterials for Photocatalytic Fuel Generations. *Chem. Rev.*, 2014, 114, 9987–10043.

99. D. Kang, T. W. Kim, S. R. Kubota, A. C. Cardiel, H. G. Cha and K. S. Choi, Electrochemical Synthesis of Photoelectrodes and Catalysts for Use in Solar Water Splitting. *Chem. Rev*., 2015, 115, 12839–12887.

100. H. Tong, S. Ouyang, Y. Bi, N. Umezawa, M. Oshikiri and J. Ye, Nano-photocatalytic Materials: Possibilities and Challenges. *Adv. Mater.*, 2012, 24, 229–251.

101. J. Ran, J. Zhang, J. Yu, M. Jaroniec and S. Z. Qiao, Earth-abundant cacatalysts for semiconductor-based photocatalytic water splitting. *Chem. Soc. Rev.*, 2014, 43, 7787–7812.

102. X. Chang, T. Wang, P. Zhang, J. Zhang, A. Li and J. Gong, Enhanced Surface Reaction Kinetics and Charge Separation of P-n Heterojunction Co_3O_4/$BiVO_4$ Photoanodes. *J. Am. Chem. Soc*., 2015, 137, 8356–8359.

103. Khatib, A.K., Earlougher, R.C., Kantar, K. CO_2 Injection Asanimmiscible application for enhanced recovery in heavy oil reservoirs. *Society of Petroleum Engineers*; 1981.

104. Zhang, N., Wei, M., & Bai, B. (2018). Statistical and analytical review of worldwide CO_2 immiscible field applications. *Fuel*, 220, 89–100.

105. Hashimoto, K., Yamasaki, M., Meguro, S., Sasaki, T., Katagiri, H., Izumiya, K., Kumagai, N., Habazaki, H., Akiyama, E., Asami, K. (2002). Materials for global carbon dioxide recycling. *Corrosion Science*, 44(2), 371–386.

106. J. Gao, Y. Wang, Y. Ping, D. Hu, G. Xu, F. Gu and F. Su, A thermodynamic analysis of methanation reactions of carbon oxides for the production of synthetic natural gas. *RSC Adv.*, 2012, 2, 2358.

107. F. Koschany, D. Schlereth and O. Hinrichsen, On the kinetics of the methanation of carbon dioxide on coprecipitated $NiAlO_x$. *Appl. Catal., B*, 2016, 181, 504–516.

108. Li, W., Wang, H., Jiang, X., Zhu, J., Liu, Z., Guo, X., & Song, C. (2018). A short review of recent advances in CO_2 hydrogenation to hydrocarbons over heterogeneous catalysts. *RSC Adv.*, 8(14), 7651–7669.

109. Audi steps up research into synthetic fuels. Audi MediaCenter. Available at: https://www.audi-mediacenter.com/en/press-releases/audi-steps-up-research-into-synthetic-fuels-9546

110. H. H. Shin, L. Lu, Z. Yang, C. J. Kiely and S. McIntosh, Cobalt Catalysts Decorated with Platinum Atoms Supported on Barium Zirconate Provide Enhanced Activity and Selectivity for CO_2 Methanation. *ACS Catal.*, 2016, 6, 2811–2818.

111. I. Rossetti, C. Biffi, C. L. Bianchi, V. Nichele, M. Signoretto, F. Menegazzo, E. Finocchio, G. Ramis and A. Di Michele, Ni/SiO_2 and Ni/ZrO_2 catalysts for the steam reforming of ethanol. *Appl. Catal., B*, 2012, 117–118, 384–396.

112. D. Theleritis, S. Souentie, A. Siokou, A. Katsaounis and C. G. Vayenas, Hydrogenation of CO_2 over Ru/YSZ Electropromoted Catalysts. *ACS Catal*., 2012, 2, 770–780.

113. J. H. Kwak, L. Kovarik and J. Szanyi, CO_2 Reduction on Supported Ru/Al_2O_3 Catalysts: Cluster Size Dependence of Product Selectivity. *ACS Catal*., 2013, 3, 2449–2455.

114. A. Karelovic and P. Ruiz, CO_2 hydrogenation at low temperature over $Rh/\gamma\text{-}Al_2O_3$ catalysts: Effect of the metal particle size on catalytic performances and reaction mechanism. *Appl. Catal*., B, 2012, 113–114, 237– 249.

115. J. N. Park and E. W. McFarland, A highly dispersed $Pd\text{-}Mg/SiO_2$ catalyst active for methanation of CO_2. *J. Catal.*, 2009, 266, 92–97.

116. J. H. Kwak, L. Kovarik and J. Szanyi, Heterogeneous Catalysis on Atomically Dispersed Supported Metals: CO_2 Reduction on Multifunctional Pd Catalysts. *ACS Catal*., 2013, 3, 2094–2100.

117. M. Younas, L. L. Kong, M. J. K. Bashir, H. Nadeem, A. Shehzad and S. Sethupathi, Recent Advancements, Fundamental Challenges, and Opportunities in Catalytic Methanation of CO_2. *Energy Fuels*, 2016, 30, 8815–8831.

118. G. Du, S. Lim, Y. Yang, C. Wang, L. Pfefferle and G. L. Haller, Methanation of carbon dioxide on Ni-incorporated MCM-41 catalysts: The influence of catalyst pretreatment and study of steady-state reaction. *J. Catal*., 2007, 249, 370–379.

119. D. C. Upham, A. R. Derk, S. Sharma, H. Metiu and E. W. McFarland, CO_2 methanation by Ru-doped ceria: the role of the oxidation state of the surface. *Catal. Sci. Technol*., 2015, 5, 1783–1791.

120. R. Razzaq, C. Li, M. Usman, K. Suzuki and S. Zhang, A highly active and stable $CO_4N/\gamma\text{-}Al_2O_3$ catalyst for CO and CO_2 methanation to produce synthetic natural gas (SNG). *Chem. Eng. J.*, 2015, 262, 1090–1098.

121. M. A. A. Aziz, A. A. Jalil, S. Triwahyono, R. R. Mukti, Y. H. Taufiq -Yap and M. R. Sazegar, Highly active Ni-promoted mesostructured silica nanoparticles for CO_2 methanation. *Appl. Catal., B*, 2014, 147, 359–368.

122. G. R. Johnson and A. T. Bell, Role of ZrO_2 in Promoting the Activity and Selectivity of Co-Based Fischer-Tropsch Synthesis Catalysts. *ACS Catal.*, 2016, 6, 100–114.

123. G. Zeng, J. Qiu, Z. Li, P. Pavaskar and S. B. Cronin, CO_2 Reduction to Methanol on TiO_2-Passivated GaP Photocatalysts. *ACS Catal.*, 2014, 4, 3512–3516.

124. G. Zhou, H. Liu, K. Cui, H. Xie, Z. Jiao, G. Zhang, K. Xiong and X. Zheng, Methanation of carbon dioxide over Ni/CeO_2 catalysts: Effects of support CeO_2 structure. *Int. J. Hydrogen Energy*, 2017, 42, 16108– 16117.

125. A. Kim, C. Sanchez, G. Patriarche, O. Ersen, S. Moldovan, A. Wisnet, C. Sassoye and D. P. Debecker, Selective CO_2 methanation on Ru/TiO_2 catalysts: unravelling the decisive role of the TiO_2 support crystal structure. *Catal. Sci. Technol.*, 2016, 6, 8117–8128.

126. H. C. Wu, Y. C. Chang, J. H. Wu, J. H. Lin, I. K. Lin and C. S. Chen, Methanation of CO_2 and reverse water gas shift reactions on Ni/SiO_2 catalysts: the influence of particle size on selectivity and reaction pathway. *Catal. Sci. Technol.*, 2015, 5, 4154–4163.

127. S. Kattel, P. Liu and J. Chen, Tuning Selectivity of CO_2 Hydrogenation Reactions at the Metal/Oxide Interface. *J. Am. Chem. Soc.*, 2017, 139, 9739–9754.

128. F. Wang, S. He, H. Chen, B. Wang, L. Zheng, M. Wei, D. G. Evans and X. Duan, Active Site Dependent Reaction Mechanism over Ru/CeO_2 Catalyst toward CO_2 Methanation. *J. Am. Chem. Soc.*, 2016, 138, 6298–6305.

129. S. Sharma, K. B. Sravan Kumar, Y. M. Chandnani, V. S. Phani Kumar, B. P. Gangwar, A. Singhal and P. A. Deshpande, Mechanistic Insights into CO_2 Methanation over Ru-Substituted CeO_2. *J. Phys. Chem. C*, 2016, 120, 14101– 14112.

130. W. Li, X. Nie, X. Jiang, A. Zhang, F. Ding, M. Liu, Z. Liu, X. Guo and C. Song, ZrO_2 support imparts superior activity and stability of Co catalysts for CO_2 methanation. *Appl. Catal., B*, 2018, 220, 397–408.

131. Duyar, M. S., Ramachandran, A., Wang, C., & Farrauto, R. J. (2015). Kinetics of CO_2 methanation over Ru/γ-Al_2O_3 and implications for renewable energy storage applications. *Journal of CO_2 Utilization*, 12, 27–33.

132. Şener, Ş. E. C., Sharp, J. L., & Anctil, A. (2018). Factors impacting diverging paths of renewable energy: A review. *Renewable and Sustainable Energy Reviews*, 81, 2335–2342.

133. Barriers to Renewable Energy Technologies. Union of Concerned Scientists, Science for a Healthy Planet and Safer World. Available at: https://www.ucsusa.org/clean-energy/renewable-energy/barriers-to-renewable-energy#.Wqb6sJPwYWo

134. McCabe, A., Pojani, D., & van Groenou, A. B. (2018). The application of renewable energy to social housing: A systematic review. *Energy Policy*, 114, 549–557.

135. Mohsin, M., Rasheed, A. K., & Saidur, R. (2018). Economic viability and production capacity of wind generated renewable hydrogen. *International Journal of Hydrogen Energy*, 43(5), 2621–2630.

136. Rachchh R, Kumar M, Tripathi B. Solar photovoltaic system design optimization by shading analysis to maximize energy generation from limited urban area. *Energy Convers. Manag*. 2016;115:244–52.

137. Zhu W, Deng Y, Wang Y, Shen S, Gulfam R. High-performance photovoltaic-thermoelectric hybrid power generation system with optimized thermal management. *Energy* 2016;100:91–101.

138. Fereidooni, M., Mostafaeipour, A., Kalantar, V., & Goudarzi, H. (2018). A comprehensive evaluation of hydrogen production from photovoltaic power station. *Renewable and Sustainable Energy Reviews*, 82, 415–423.

139. Gruene, P., Belova, A. G., Yegulalp, T. M., Farrauto, R. J., & Castaldi, M. J. (2011). Dispersed Calcium Oxide as a Reversible and Efficient CO_2 −Sorbent at Intermediate Temperatures. *Industrial & Engineering Chemistry Research*, 50(7), 4042–4049.

140. Janke, C., Duyar, M. S., Hoskins, M., & Farrauto, R. (2014). Catalytic and adsorption studies for the hydrogenation of CO_2 to methane. *Applied Catalysis B: Environmental*, 152–153(1), 184–191.

141. Zheng, Q., Farrauto, R., & Chau Nguyen, A. (2016). Adsorption and Methanation of Flue Gas CO_2 with Dual Functional Catalytic Materials: A Parametric Study. *Industrial and Engineering Chemistry Research*, 55(24), 6768–6776.

142. Eliche-Quesada, D., Mérida-Robles, J. M., Rodríguez-Castellón, E., & Jiménez-López, A. (2005). Ru, Os and Ru–Os supported on mesoporous silica doped with zirconium as mild thio-tolerant catalysts in the hydrogenation and hydrogenolysis/hydrocracking of tetralin. *Applied Catalysis A: General*, 279(1), 209–221.

143. Tian, P., Blanchard, J., Fajerwerg, K., Breysse, M., Vrinat, M., & Liu, Z. (2003). Preparation of Ru metal nanoparticles in mesoporous materials: Influence of sulfur on the hydrogenating activity. *Microporous and Mesoporous Materials*, 60(1–3), 197–206.

144. Nguyen, T. S., Lefferts, L., Sai Sankar Gupta, K. B. and Seshan, K. (2015), Catalytic Conversion of Biomass Pyrolysis Vapours over Sodium-Based Catalyst: A Study on the State of Sodium on the Catalyst. *Chem. Cat. Chem.*, 7: 1833–1840.

145. Islam, A.; Ravindra, P.; *Biodiesel Production with Green Technologies*; Springer International Publishing Switzerland: Cham, Switzerland, 2017; Chapter 1.

146. Batholomew, C.; Farrauto, R.J. *Fundamentals of Industrial Catalytic Processes*; Wiley and Sons: New York, NY, USA, 2006; Chapter 10.

147. Bartholomew, C.H.; Farrauto, R.J. Chemistry of nickel-alumina catalysts. *J. Catal*.1976, 45, 41–53.

148. Wang, S., Schrunk, E. T., Mahajan, H., & Farrauto, R. J. (2017). The Role of Ruthenium in CO_2 Capture and Catalytic Conversion to Fuel by Dual Function Materials (DFM). *Catalysts*, 7(3), 88.

149. Keturakis, C. J., Ni, F., Spicer, M., Beaver, M. G., Caram, H. S., & Wachs, I. E. (2014). Monitoring Solid Oxide CO_2 Capture Sorbents in Action. *Chem. Sus. Chem*., 7(12), 3459–3466.

150. Kawano, K., Kosuge, H., Oshima, N., & Funakubo, H. (2007). Low-Temperature Preparation of Metallic Ruthenium Films by MOCVD Using Bis (2,4-dimethylpentadienyl) ruthenium. *Electrochemical and Solid State Letters* 2007, 10, D60-D62.